Chem Soc Rev

TUTORIAL REVIEW

View Article Online
View Journal | View Issue

Cite this: *Chem. Soc. Rev.*, 2022, **51**, 5300

Photochemistry of transition metal carbonyls

James J. Turner,*[a] Michael W. George,[a] Martyn Poliakoff[a] and Robin N. Perutz*[b]

The purpose of this Tutorial Review is to outline the fundamental photochemistry of metal carbonyls, and to show how the advances in technology have increased our understanding of the detailed mechanisms, particularly how relatively simple experiments can provide deep understanding of complex problems. We recall some important early experiments that demonstrate the key principles underlying current research, concentrating on the binary carbonyls and selected substituted metal carbonyls. At each stage, we illustrate with examples from recent applications. This review first considers the detection of photochemical intermediates in three environments: glasses and matrices; gas phase; solution. It is followed by an examination of the theory underpinning these observations. In the final two sections, we briefly address applications to the characterization and behaviour of complexes with very labile ligands such as N_2, H_2 and alkanes, concentrating on key mechanistic points, and also describe some principles and examples of photocatalysis.

Received 25th March 2022

DOI: 10.1039/d1cs00826a

rsc.li/chem-soc-rev

Key learning points

(1) On absorption of one UV/vis photon, binary metal carbonyls usually undergo loss of a single CO group in solution or matrices, but loss of several CO groups in the gas phase.

(2) Photodissociation of CO normally occurs within <1 picosecond of light absorption, such that there is no time for excited states to equilibrate with their surroundings.

(3) In substituted metal carbonyls and metal–metal bonded carbonyls, there are often two competing photochemical pathways and their relative quantum yields depend on the wavelength of irradiation, indicating the importance of careful selection of photolysis wavelengths.

(4) The coordinatively unsaturated metal carbonyls formed by photodissociation are highly reactive and coordinate a solvent molecule, including alkanes and noble gases, within a few picoseconds. These alkane complexes act as stores of the fragments until the final photoproducts are formed; they also act as test-beds for understanding metal–ligand bonding.

(5) Photodissociation of CO occurs by initial excitation into metal-to-CO charge-transfer excited states followed by rapid crossing into ligand-field (d–d) excited states. The excited states are typically spin-singlets but the ground states of some 3d transition metal fragments are spin-triplets.

1. Introduction

1.1 Previous reviews and applications of metal carbonyl photochemistry

Transition metal carbonyls combine great photosensitivity and extraordinary reporters in the form of their CO-stretching bands with their structure sensitivity and exceptionally large absorption coefficients. In 1974, Mark Wrighton, one of the pioneers of the topic, published a review[1] entitled "The Photochemistry of Metal Carbonyls" which summarised all aspects of the subject known at the time. A more recent review has emphasised the photophysical processes.[2] The purpose of this Tutorial Review is to outline some of this basic photochemistry, draw out the principles, show how the advances in technology have increased our understanding of the detailed mechanisms, and to highlight how the simpler approaches used in early days can shed light on the more sophisticated modern problems.

Photochemistry is applied in such areas as synthesis, photochemical CO-releasing molecules (photoCORMs), photocatalysis, photopolymerisation and photochemical modification of surfaces and glasses. In each of these examples, a basic understanding of the subtleties of metal carbonyl photochemistry is a prerequisite. It has also been crucial in understanding the ability of noble gases and alkanes to form labile bonds to transition metals.

A striking example of photosubstitution is the recent synthesis of a new boron complex by photolysis of $(OC)_5Cr{=}B(aryl)$ (aryl = 2,6-(2,4,6-$^{i}Pr_3C_6H_2)_2C_6H_3$) in the presence of diphenylacetylene (Scheme 1).[3] The interesting feature of the product is

[a] School of Chemistry University of Nottingham, NG7 2RD, UK. E-mail: james.turner@nottingham.ac.uk
[b] Department of Chemistry, University of York, York, YO10 5DD, UK. E-mail: robin.perutz@york.ac.uk

that it contains the borirene group (isoelectronic with the cyclopropenium cation) attached to a single metal centre. Photosubstitution also provides a route to very labile complexes (Section 6) exemplified by the publication during revision of this review of a methane complex at low temperature that could be characterised by ^{13}C and ^{1}H NMR in a fluorocarbon solvent (Scheme 2).[4]

Carbon monoxide is toxic but, surprisingly, it has very important biological functions.[5] Current research focuses on how to make compounds which can release CO in the body in a controlled manner as a therapeutic agent. PhotoCORMs use transition metal carbonyls which can eject CO on photolysis.[6] CO ejection usually requires UV light, which is somewhat dangerous, and anyway has low skin penetration. One way round this is to use a substituted species that absorbs in the visible such as $(CO)_5ReMn(CO)_3$(phenanthroline)[7] which under deep-red photolysis splits the Re–Mn bond to give mononuclear radicals; normally these would simply recombine but in oxygenated media, species are formed which are much more labile towards CO release. In another example, $MnBr(CO)_3(L)$ (L = phenol substituted terpyridyl),[8] the rate of photorelease can be regulated through deprotonation by F^- that red-shifts the absorption dramatically. A different approach is to use a palladium porphyrin as a photosensitiser which on absorption at 635 nm converts to the excited triplet state, $^{3}Pd(porph)^*$; the latter transfers energy to $Mn_2(CO)_{10}$ exciting it to a photolabile triplet state, releasing CO.[9] This is intriguing because almost all photochemistry of metal carbonyls occurs from excited singlet states and triplet sensitisation is a rarity.

James J. Turner

In 1960, Jim Turner obtained his PhD on NMR with Norman Sheppard in Cambridge. Following two years as a Harkness Fellow in California, learning about matrix isolation with George Pimentel, he returned to Cambridge as Fellow of King's College and University Lecturer. He subsequently held Professorships at Newcastle on Tyne and Nottingham where he is now Emeritus and still active in research. For most of his career he has been interested in the structure, dynamics and photochemical behaviour of transition metal carbonyls, their fragments, intermediates and excited states. He has collaborated closely with the other three authors of this Review. He was elected to the Royal Society in 1992.

Michael W. George

Michael W. George, Professor of Chemistry at the University of Nottingham, obtained his PhD with Martyn Poliakoff in Nottingham and has since collaborated with all three authors of this review. He applies photochemistry combined with time-resolved infrared spectroscopy and XAFS over femtoseconds to seconds, to unravel the complexities of excited states and reaction mechanisms of transition metal compounds. He drove the initial development of TRIR instruments at the Rutherford Appleton Laboratory. In addition he harnesses light for the more efficient manufacture of chemicals using continuous photochemistry and electrosynthesis. He is a member of Academia Europaea and received the 2021 IRDG Norman Sheppard Award and the 2022 RSC Interdisciplinary Prize.

Martyn Poliakoff

Martyn Poliakoff was born in London and spent over 30 years collaborating with Jim Turner on carbonyl photochemistry before moving into the then new field of applying supercritical fluids to Green Chemistry. After his PhD in Cambridge with Jim, Martyn spent 7 years at Newcastle University. Since 1979, he has worked at Nottingham where he is now Research Professor of Chemistry, currently working on continuous chemical processing in a project led by Mike George. He served as Foreign Secretary of the Royal Society, the UK's national academy of science, (2011–2016). He is one of the presenters of the YouTube Chemistry Channel, ***https://www.periodicvideos.com.***

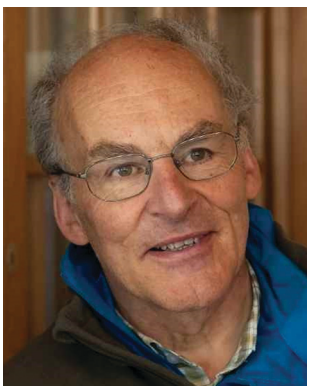

Robin N. Perutz

After a PhD under Jim Turner in Cambridge and Newcastle, Robin Perutz worked in Mülheim, Edinburgh and Oxford before moving to the University of York in 1983 where he is now an emeritus professor. Robin studies photochemical reactions of transition metal compounds in order to understand catalysis and develop solar energy. He has received prizes from RSC and is a Fellow of the Royal Society. For many years Robin has been active in the women in science agenda and in supporting students with disabilities.

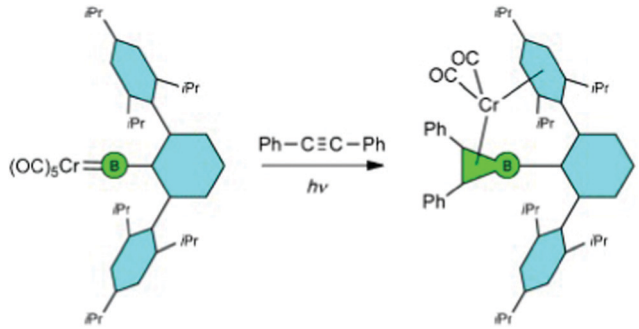

Scheme 1 Application of photosubstitution to synthesise borirene complex. Reproduced with permission from H. Braunschweig, R. D. Dewhurst, K. Radacki, C. W. Tate and A. Vargas, *Angew. Chem., Int. Ed.*, 2014, **53**, 6263–6266, copyright Wiley and Son 2014.[3]

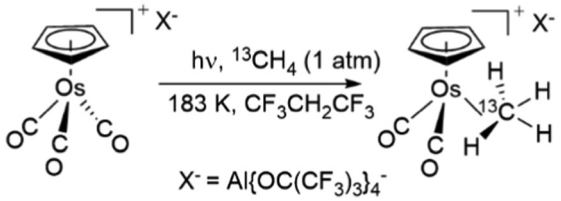

Scheme 2 Formation of osmium methane complex[4] by photosubstitution.

In photocatalysis, the photon energy can be used to drive the reaction uphill or to release (also described as ''uncage'') the active catalyst (Section 7). Additionally, photochemical initiation of a reaction can elucidate the mechanism of a thermal catalytic reaction. A recent example concerns the reaction of 2-phenylpyridine (ppy) with alkynes to form alkenylated products, catalysed by manganese carbonyl complexes at elevated temperature and proceeding *via* cyclomanganated intermediates. The mechanism of the C–H bond functionalization is unravelled with time-resolved IR examination of the photochemistry of $Mn(CO)_4(ppy)$ (Scheme 3).[10] Materials applications are illustrated by a study of a range of metal carbonyls in the radical photopolymerisation of vinylidene fluoride.[11]

Surface modification is illustrated by the photolysis of $Cr(CO)_6$ in CH_3CN on graphene proposed to lead *via* $Cr(CO)_3(CH_3CN)_3$ to (η^6-graphene)$Cr(CO)_3$ with greatly increased conductivity compared to graphene.[12] Look and Gafney have employed photolysis of $W(CO)_6$ adsorbed on Vycor glass to generate photochromic tungsten oxides that are then used for photocatalytic reduction of CO_2.[13]

This tutorial review concentrates on the binary carbonyls and cyclopentadienyl derivatives, $M(CO)_6$ (M = Cr, Mo, W), $Fe(CO)_5$, $CpM(CO)_n$ (M = Nb, Mn, Re, Co, Rh, Cp = η^5-C_5H_5), $Mn_2(CO)_{10}$ and $[CpFe(CO)_2]_2$. Through restricting ourselves to

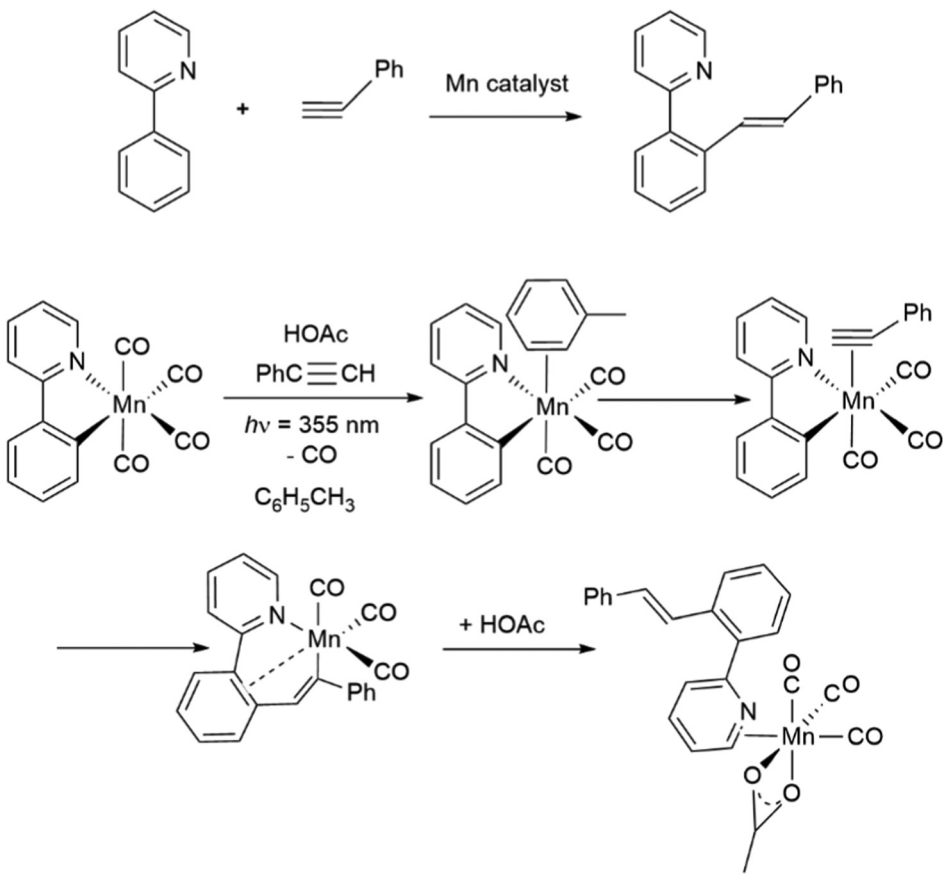

Scheme 3 Above: Catalytic reaction. Below: Intermediates detected in the Mn(I) carbonyl-catalysed C–H bond functionalization of 2-phenylpyridine by TRIR spectroscopy. Adapted with permission from *J. Am. Chem. Soc.*, 2021, **143**, 1356–1364. Copyright 2021, American Chemical Society.[10]

these examples, we exemplify the fundamental principles of dissociative photochemistry. Alternative pathways of formation of equilibrated excited states are limited to certain substituted metal carbonyls and are mentioned only briefly.

To unravel the photochemistry, several approaches are usually needed. We first concentrate on identifying the initial products by looking at the behaviour in low-temperature glasses and matrices (Section 2), in the gas phase (Section 3) and in solution (Section 4). This is followed by a theory and dynamics section (Section 5) where we compare the predictions of theory and the experimental observations. The very first step in the photochemistry involves excited states and we consider how the photoproducts arise from specific excited states. Finally, we look at applications for the synthesis of photoproducts with very labile ligands (Section 6) and photocatalysis (Section 7).

1.2 Essential principles of IR spectroscopy

Much of the underpinning of metal carbonyl photochemistry is best served by the application of IR spectroscopy to C–O vibrations. These IR ν(C–O) bands are extremely intense, usually well-separated (at about 2000 cm^{-1}) from other molecular vibrations and are narrow in solution in non-polar solvents, although in polar solvents they are broader.[14] Two further aspects of the solvent need to be considered, namely its inherent reactivity and its own IR absorbance in the C–O stretching region.

One approach that we introduced involves the use in metal carbonyl photochemistry, of liquefied noble gases, mostly Xe and Kr, as solvents at low temperature[15] and as supercritical solvents[16] near room temperature. These solvents have no IR absorptions, and hence allow the use of long pathlengths to compensate for the low solubility of the precursor complexes. The high solubility of CO, N_2, H_2 and other gases allows studies of reactivity with these species (see Section 6). With pressures up to 10 bar (Table 1), it is possible to cover a wide temperature range by use of liquid Ar, Kr and Xe. With supercritical solvents, it is even possible to reach room temperature. In principle such solvents should provide an ''innocuous'' environment, but, as we shall see, there can be interesting interactions.

The C–O frequencies can be interpreted by the Energy Factored Force Field (EFFF), which was first exploited by Cotton and Kraihanzel.[17] A reminder of the principles is appropriate.[18] In this approach, it is assumed that the C–O stretching vibrations can be treated separately from the other molecular vibrations. The spectra are strongly influenced by the electronic coupling between CO groups, but all other electronic and mechanical coupling can be ignored. When compared with a complete force constant analysis,[19] the principal force constants (k_{CO}) are very similar to the (anharmonic) full analysis constants (F_{CO}); the major difference is in the interaction constants ($k_{CO,CO}$ compared with $F_{CO,CO}$). This approximation had its critics,[19] but the EFFF works amazingly well in applications to structure and bonding,[20,21] as we shall see. Moreover, the patterns of CO-stretching frequencies give information about the symmetry of the molecule and the number of CO groups. Where the spectra with natural abundance isotopes do not resolve ambiguities, a decisive conclusion can be reached by isotopic substitution ($^{13}C^{16}O$ or $^{12}C^{18}O$). The EFFF is extremely powerful in conjunction with relative intensities (I) for estimation of C–M–C bond angles;[18] for simple structures the angles are given by:

$$M(CO)_2\text{: } I(\text{sym})/I(\text{antisym}) = \tan^2(\theta/2) \quad (\theta = \text{C–M–C angle})$$

$$M(CO)_3\ (C_{3v})\text{: } I(a_1)/I(e) = [3\cot^2(\theta/2) - 1]/4 \quad (\theta = \text{C–M–C angle})$$

$$M(CO)_4\ (C_{4v})\text{: } I(a_1)/I(e) = 2\tan^2\phi \quad (\phi = \text{angle of droop})$$

If the symmetry of these molecules is lower, or if one or more ^{12}COs are replaced by ^{13}COs, the relationships are more complex, but still soluble.

How do the force constants, and hence frequencies, of metal carbonyls vary? In the light of both high-level and DFT approaches in recent years, the EFFF has become less fashionable. However, although modern theoretical calculations can predict structures and energetics reasonably well, they are less reliable, even with 'adjustments', when it comes to predicting frequencies. Thus we argue there is still a role for the simple approach.

As a reminder, Fig. 1 shows the bonding of CO to a transition metal in the Dewar–Chatt–Duncanson model. The σ donor orbital slightly C–O antibonding, and the π acceptor orbital is strongly C–O antibonding. The changes in the force constants determined by EFFF can be interpreted through this model. There can be considerable argument as to whether σ or π bonding is more important in affecting the C–O bond strength and hence the C–O force constant, but some general points remain.

Table 1 Properties of noble gases

Noble gas	Melting point (K)	Temp. (K) of liquid with vapour pressure of 10 bar	Critical temp. (K)	Critical pressure (bar)
Ar	84	116	151	49
Kr	116	159	209	55
Xe	161	219	290	58

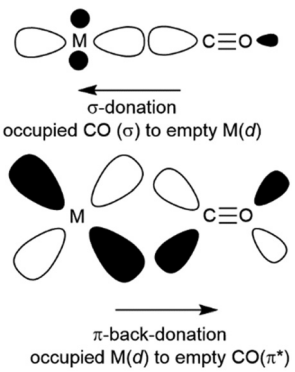

Fig. 1 Dewar–Chatt–Duncanson scheme for bonding of CO to a transition metal.

The σ/π properties of other ligands will have an effect. For example in the classic work of Tolman,[22] the a_1 frequency of the CO groups in $Ni(CO)_3$(phosphine) complexes increased from 2056 cm^{-1} in the essentially σ donating P(*t*-butyl)$_3$ complex to 2111 cm^{-1} in the π-accepting ligand PF_3 complex, where the back donation to PF_3 relieves the back-bonding pressure on the CO groups, so that the C–O frequency increases. Force constants provide an effective way of comparing bond strengths that is independent of the molecular symmetry and number of CO groups. They are especially valuable for comparisons of π-acceptor properties of ligands. DFT calculations provide a direct route to estimating CO-stretching frequencies but the connection to force constants is usually lost and bond strength is approached in very different ways.

The Tolman approach was further developed by Gusev,[23] who showed that there is a close correlation between experimental and DFT calculated frequencies for the $Ni(CO)_3L$ series, although the calculated frequencies were some 100 cm^{-1} different from the experimental. He also obtained a good correlation between experimental frequencies and DFT calculated C–O bond distances. The closely connected relationship between M–C and C–O distances has been analysed by Hocking and Hambley providing more detailed bonding indicators.[24]

We note that the ν(CO) will increase with:

(a) Positive charge on the complex (about 100 cm^{-1} per unit of charge);

(b) Increasing number of CO groups (about 30 cm^{-1} per added CO group);

(c) Oxidation state of the metal (about 20–40 cm^{-1} for an increase of 1 unit);

A very useful way of predicting the EFFF C–O force constants (k_{CO}) – and hence ν(CO) – was introduced by John Timney (eqn (1)):[25]

$$k_{CO} = k_d + \sum \varepsilon_L^{\theta} \quad (1)$$

The parameter k_d is the force constant for the isolated monocarbonyl of a metal M(CO); ε_L^{θ} is the 'ligand effect constant' for ligand L at an angle θ to the C–O group being considered. Thus for the tetrahedral complex $Ni(CO)_3(PH_3)$, we have (eqn (2)):

$$k_{CO} = k_{Ni} + 2\varepsilon_{CO}^{109.5} + \varepsilon_{PH3}^{109.5} \quad (2)$$

Values of k_d for metals and ε for a series of ligands were provided. To predict a C–O IR spectrum, it is necessary to have C–O/C–O interaction constants and relationships were described to estimate these. As an example of the application of this method, it was possible to correct the assignment of the spectra of the series $Ni(CO)_{4-x}(N_2)_x$, and hence to make more sense of the bonding.[26]

1.3 Time-resolved infrared spectroscopy (TRIR)

Most modern Fourier Transform IR (FTIR) instruments have a spectral resolution of at least 0.5 cm^{-1}, easily adequate for most purposes for 'static' or slowly changing systems, but alternative methods are required for systems that evolve in less than *ca.* 0.1 s. To follow photochemical changes, it is necessary to provide time-resolved spectra. The understanding of metal carbonyl photochemistry has been transformed by fast time-resolved IR spectroscopy (TRIR), enabled by a short pulse of pump light source to initiate a chemical reaction and to generate a high concentration of transient species. A second beam (the probe beam) passes through the sample to monitor changes that occur following the pump. Thus TRIR probes reaction dynamics and characterizes reactive intermediates on timescales that are inaccessible to conventional spectroscopy. Moreover, TRIR provides the structure sensitivity that is lacking in time-resolved UV/visible absorption. The first measurements in the mid-infrared used rapid-scan methods; the technique has continually advanced with new developments, particularly in lasers and computers, such that measurements can now be made right across the mid-IR on timescales from femtoseconds to milliseconds. Many approaches have been used for TRIR experiments and none has become uniformly adopted as the best because many different parameters need to be considered including: (i) the required wavenumber range; (ii) time-resolution; (iii) spectral resolution; (iv) sensitivity *i.e.*, signal-to-noise required to observe the expected change in absorbance, Δabs, following irradiation.[27]

This review includes examples spanning almost 40 years which illustrate the transformation in the key parameters. The fingerprint and other regions provide insights about other ligands bound to metal centres complementing information from the ν(CO) region.

1.3.1 The UV/visible pump source. Time-resolved spectroscopy aims to excite all the molecules simultaneously. In the early days, a flash lamp was used which restricted the timescales to milli- to microseconds. The flash lamps were soon replaced by pump lasers. Nowadays, the time range, wavelength and repetition rate of pump lasers can be matched to the spectrum of the absorber and the dynamics under study.

1.3.2 Broad-band IR sources with dispersive spectrometers. In pioneering applications of TRIR to metal carbonyl photochemistry, radiation from a hot rod (globar) was used for TRIR measurements on the microsecond timescale. The change in IR transmission at one particular IR frequency was measured following excitation with repeat measurements at different frequencies allowing the TRIR spectra to be built up "point-by-point" for any required time delay. In common with all TRIR approaches, this method requires the conditions to be repeatable for each flash. Repeatability is best achieved by replacing the solution after each flash, usually in a flow cell or by rastering the sample. In the first breakthrough, the transient CO-loss intermediate of $Cr(CO)_6$ in cyclohexane could be monitored.[28] These early TRIR spectrometers suffered from low IR photon flux, giving poor signal-to-noise ratio and poor spectral resolution.

The use of pump lasers, noise reduction techniques and computer-controlled IR scanning have resulted in commercial instruments based upon dispersive spectrometers which can record IR spectra with $\Delta abs < 10^{-5}$ on nanosecond to millisecond timescales.[29]

1.3.3 Laser IR sources with point-by-point methods (time range 10^0 to 10^{-8} s). High power cw IR laser sources enabled the dispersive methods to be massively improved. The IR probe

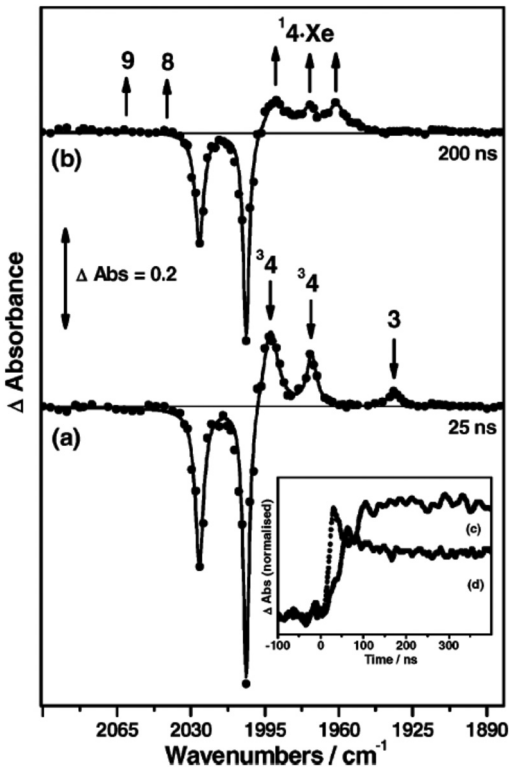

Fig. 2 TRIR difference spectra of $Fe(CO)_5$ in supercritical Xe (103 bar) doped with CO (2 bar) obtained at (a) 25 and (b) 200 ns after laser flash at 266 nm. The negative peaks correspond to loss of $Fe(CO)_5$, the positive peaks to growth of products. The peaks are labelled according to the number of CO groups. The major products are: ^{3}**4** = $^3Fe(CO)_4$; ^{1}**4-Xe** = $^1Fe(CO)_4$–Xe; **3** = $Fe(CO)_3$. In addition, traces of $Fe_2(CO)_8$ **8** and $Fe_2(CO)_9$ **9** are formed. The inset shows the kinetics of (c) the formation of ^{1}**4-Xe** at 1961 cm^{-1} and (d) the decay of ^{3}**4** overlapped with the growth of ^{1}**4-Xe** at 1990 cm^{-1}. Reproduced with permission from *J. Am. Chem. Soc.*, 2004, **126**, 10713–10720. Copyright 2004, American Chemical Society.[31]

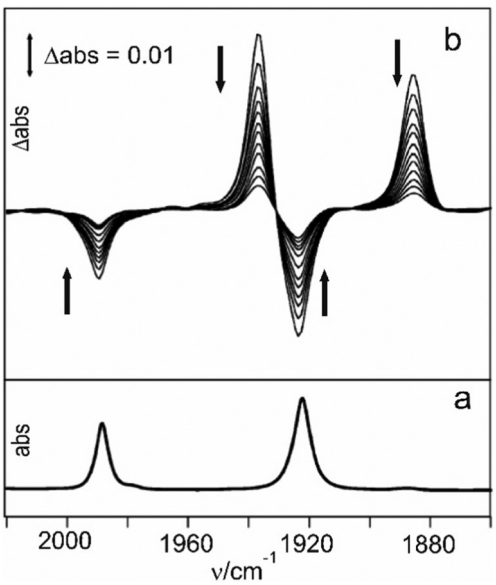

Fig. 3 (a) FTIR spectrum of $Cr(\eta^6\text{-}C_6H_6)(CO)_3$ in supercritical Xe at 298 K and 1500 psi in the presence of CO (30 psi). (b) Step scan FTIR spectra at various times between 1.0 and 2.1 μs after 355 nm laser excitation leading to the formation of $Cr(\eta^6\text{-}C_6H_6)(CO)_2Xe$. The time-resolved spectra depict the decay of the transient $Cr(\eta^6\text{-}C_6H_6)(CO)_2Xe$ and recovery of $Cr(\eta^6\text{-}C_6H_6)(CO)_3$. Reproduced from ref. 32 with permission from the Royal Society of Chemistry.

laser is tuned to one frequency at a time so generating a point-by-point TRIR spectrum. The original CO or IR diode lasers had limited frequency ranges, and the CO laser produces narrow lines separated by *ca.* 4 cm^{-1}, thus limiting the resolution. They have been superseded by External Cavity Quantum Cascade Lasers (QCLs) which deliver high power (*ca.* 0.5–1.0 W) right across the mid-IR region.[30] The photolysis of $Fe(CO)_5$ in supercritical xenon generating $^3Fe(CO)_4$ and $^1Fe(CO)_4Xe$ illustrates this method (Fig. 2, see Section 4.4).[31]

1.3.4 Broad-band IR sources with FTIR (time range 10^{-3} and 10^{-7} s). The point-by-point approach is labour-intensive. By contrast, nanosecond time-resolved step-scan Fourier transform infrared (FTIR) can cover the entire IR region by displacement of the moveable mirror of the interferometer in a step-wise manner. At each mirror position, the time-dependent change in IR intensity is measured following excitation, resulting in a series of time-dependent interferograms that are converted to the corresponding IR absorption spectra. The formation of $Cr(\eta^6\text{-}C_6H_6)(CO)_2Xe$ from $Cr(\eta^6\text{-}C_6H_6)(CO)_3$ illustrates the high quality of spectra that can be obtained (Fig. 3).[32]

Since any imperfections in the interferogram generated in step-scan are transformed into the whole spectrum, this method is less forgiving of errors in repeatability than methods described above. Consequently, time-resolved step-scan FTIR has not been as widely implemented.

1.3.5 Ultrafast methods (time range 10^{-13} to 10^{-9} s). The methods described above do not allow measurements faster than *ca.* 10 ns, but now many studies investigate times in the fs and ps region. They employ broad-band pulsed IR lasers so avoiding the point-by-point problem. Optical parametric amplifiers (OPAs) can be used to generate IR pulses by difference frequency mixing in a non-linear crystal yielding tunable IR radiation spanning several hundred wavenumbers which can be dispersed across linear IR array detectors. This method allows a broad spectral region to be probed in a single experiment. Signal averaging routinely produces highly sensitive spectrometers for fs and ps spectroscopy.[27] On this ultrafast scale, the time resolution is achieved by spatially delaying the probe pulse with respect to the pump pulse (light travels 0.30 mm in 1 ps). By repeating the experiment at a series of time delays, accurate kinetic information can be obtained. The techniques continually evolve leading to many variants of ultrafast TRIR. The results of modern ultrafast methods are illustrated by TRIR spectra obtained on photolysis of $CpMn(CO)_3$ showing formation of $CpMn(CO)_2$ in two spin states (Fig. 4, see Sections 2.2.2 and 4.4.3).[33]

Advances in pump laser technology have enabled the gap between nanosecond measurements and the ultrafast measurements to be bridged by coupling high-repetition nanosecond lasers as the pump

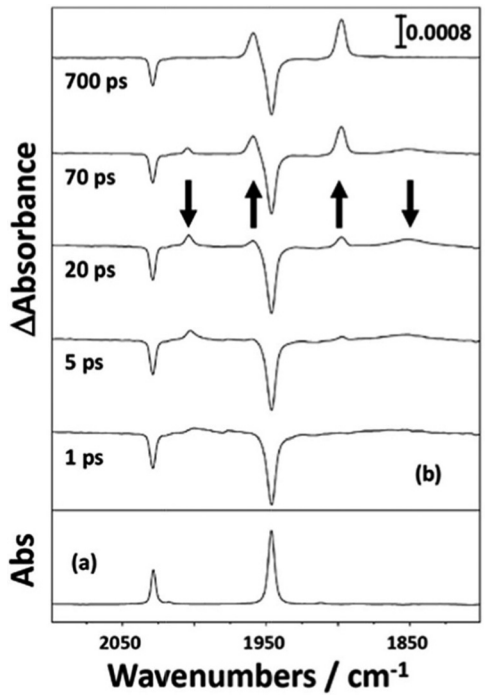

Fig. 4 (a) FTIR spectrum of a solution of $CpMn(CO)_3$ in *n*-heptane at room temperature; (b) selected picosecond TRIR spectra recorded at a series of time delays following 266 nm photolysis of the solution. Reproduced from ref. 33 with permission from the Royal Society of Chemistry.

source to these probe systems allowing TRIR measurements from sub-picosecond to milliseconds on a single spectrometer.[10]

Applications and IR spectroscopy: key points
(1) Applications: photosubstitution, photoCORMs, photocatalysis, photopolymerisation, photochemical surface modification, labile ligands.
(2) IR spectra and ν(CO) bands.
(3) Structure sensitivity: effects of charge, oxidation state, no of CO groups.
(4) Liquefied and supercritical noble gases as solvents: low reactivity, IR transparency, solubility of added gases.
(5) Energy factored force field for analysis of ν(CO).
(6) TRIR spectroscopy, key parameters: pump wavelength, IR wavenumber range, time resolution, spectral resolution, sensitivity.

2. Photochemistry in glasses and matrices

2.1 Metal hexacarbonyl photochemistry (metal = Cr, Mo, W)

2.1.1 $M(CO)_5$ species. How can you observe the first product of photodissociation of a metal carbonyl? Most stable metal carbonyls have 18-electron configurations and are coordinatively saturated. Loss of CO would generate a 16-electron coordinatively unsaturated species. Stolz *et al.* were the first to obtain spectroscopic evidence for such a species.[34,35] In these experiments, dilute solutions of $M(CO)_6$ (M = Cr, Mo, W) in 1 : 4 isopentane-methylcyclohexane were frozen to produce a colourless glass at *ca.* 90 K. UV irradiation led to the accumulation of new, yellow, species identified by the ν(CO) IR bands; for M = W at 2092 (w), 1952 (s) and 1924 (m) cm^{-1}. By comparison with known $W(CO)_5L$ IR band patterns, the bands were confidently assigned to a C_{4v} $W(CO)_5$ fragment. There was some evidence that the species was observable even as the glass melted. It is very unlikely that a 'naked' $M(CO)_5$ fragment would be so stable, implying that the species observed were actually $M(CO)_5$(alkane) (eqn (3)), improbable though this seemed at the time.

$$M(CO)_6 \xrightarrow[\text{alkane glass, 90 K M=Cr, Mo, W}]{h\nu,-CO} M(CO)_5(\text{alkane}) \qquad (3)$$

Is it possible to generate the fragments in an environment less likely to coordinate with the solvent? We turn to the technique labelled 'Matrix Isolation' by its inventor, George Pimentel.[36] In the photochemical application of this method, dilute gas mixtures of a precursor in a noble gas (Ne, Ar, Kr, Xe) are condensed onto a cold (10–20 K) IR transparent window (*e.g.* CsBr), and irradiated. In the first trial experiment[37] with a metal carbonyl, $HMn(CO)_5$ in Ar (1 : 200) was photolyzed with UV (229 nm) at 15 K. The resulting spectrum was readily assigned to $HMn(CO)_4$, but the most interesting aspect of this experiment was that irradiation with $\lambda > 285$ nm reversed the reaction (eqn (4)). This had enormous significance for future experiments, although not understood at the time. A plethora of experiments of this type followed, but we concentrate on those of particular relevance to this Tutorial.

$$HMn(CO)_5 \underset{h\nu,\ >285\,\text{nm}}{\overset{\text{Ar matrix, 15 K } h\nu,\ 229\,\text{nm}}{\rightleftharpoons}} HMn(CO)_4 + CO \qquad (4)$$

The first, partial, explanation of this reversal came in an experiment on $W(CO)_6$ which monitored the UV/vis spectrum in addition to the IR (Fig. 5).[38]

The bands labelled 6 are assigned to $W(CO)_6$; bands labelled 5 are assigned to $W(CO)_5$. Clearly a species, easily assigned as $W(CO)_5$,† is converted back to $W(CO)_6$ when it absorbs radiation in its band at 435 nm (eqn (5)). An absorption band at much longer wavelength than that of the precursor turned out to be typical of coordinatively unsaturated metal carbonyls (see Section 5). What is not clear is how the recombination works; is it simply because the absorbed radiation is transferred to the matrix, warming it locally around the $W(CO)_5$ fragment and hence causing a thermal back reaction, or is it a more specific photochemical process? One way to answer this question would be to warm the matrix and see if a back reaction occurs. However, one of the disadvantages of using frozen noble gases is that, in contrast to glasses, it is not possible to follow reactions over more than a small temperature range before

† Although the IR bands are very sharp – important in determining structure with ^{13}CO enrichment (see below) – the single t_{1u} band of $W(CO)_6$ actually appears as a doublet. This 'matrix splitting' arises in many matrix spectra and is due to multiple or unsymmetric environments in the matrix. The effect is largely understood and can be accommodated in the interpretation of the spectra.

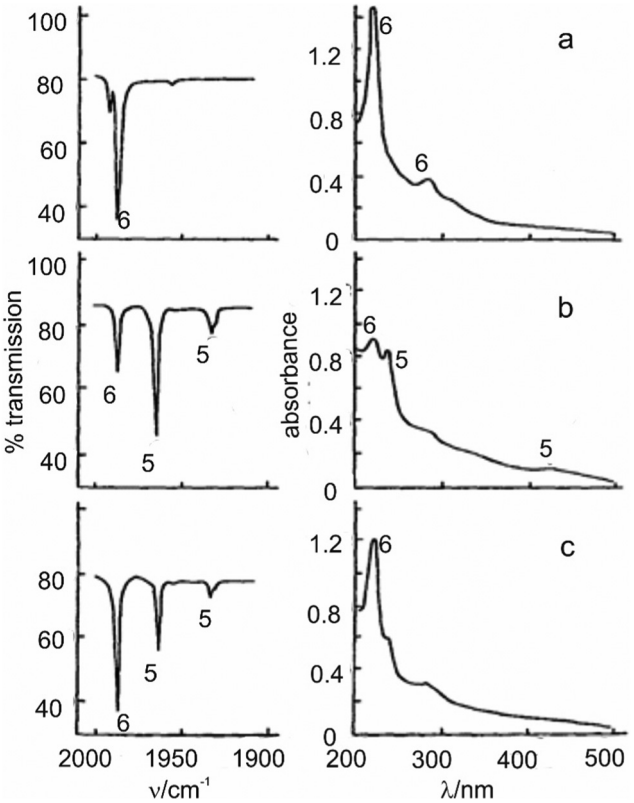

Fig. 5 IR (left) and UV/visible (right) spectra (a) of $W(CO)_6$ in argon (1/250) after depositing on to a KBr window at 20 K; (b) after 30 s photolysis with unfiltered UV light; (c) after 90 s irradiation with light >330 nm. 6 = $W(CO)_6$, 5 = $W(CO)_5$. Note the depletion of $W(CO)_5$ and recovery of $W(CO)_6$ in spectra (c). Reproduced from ref. 38 with permission from the Royal Society of Chemistry.

the matrix gas boils off. We shall later briefly consider some methods which overcome this limitation.

$$WCO_6 \underset{h\nu,\ >330\ \text{nm}}{\overset{\text{Ar matrix, 20 K } h\nu,\text{ UV unfiltered}}{\rightleftharpoons}} \underset{\lambda_{max}\ 435\ \text{nm}}{W(CO)_5 + CO} \qquad (5)$$

It is of course possible that the three C–O IR bands are wrongly assigned to $W(CO)_5$; the only way to be sure of the assignment is to substitute some of the ^{12}CO groups with ^{13}CO. For the C_{4v} $M(CO)_5$ fragment there are three IR-active frequencies (a_1, e and a_1) but five EFFF constants: the principal k_{CO}^{axial}, k_{CO}^{eq}, and the interaction $k_{CO,CO}^{eq,eq(cis)}$, $k_{CO,CO}^{eq,eq(trans)}$ and $k_{CO,CO}^{ax,eq}$ (Fig. 6). Thus the problem is underdetermined. However, with ^{13}CO substitution, more frequencies are generated, but the force constants remain the same, and the problem is, if anything, overdetermined. Employing this approach, the photogenerated fragments were shown, unquestionably, to be $M(CO)_5$ (M = Cr, Mo, W) with C_{4v} structures[39] in both Ar and CH_4 matrices. Moreover, from the relative intensities of the IR bands, it was possible to estimate that the axial/equatorial C_{ax}–M–C_{eq} bond angles were between 90° and 94°.

However, things are not so simple: the position of the visible absorption band is very sensitive to the matrix material.[40] For example with $Cr(CO)_5$, the bands occur at 624 (Ne), 533 (Ar),

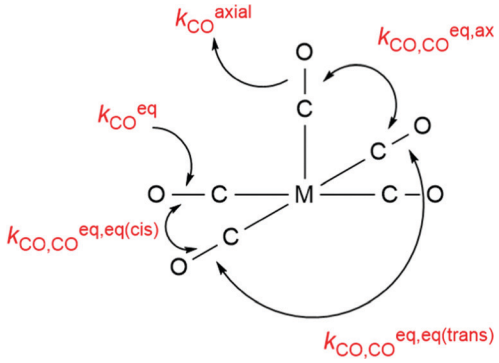

Fig. 6 Force constant definitions for C_{4v} $M(CO)_5$.

518 (Kr), 492 (Xe), and at 489 nm (CH_4); meanwhile the position of the IR bands is hardly affected. Experiments in mixed matrices, particularly of Ne and Xe, proved that two independent species were present and could be interconverted by selective photolysis; the shift in the visible band was caused by the interaction of the noble gas with the empty coordination site of the $M(CO)_5$ fragment. This leads to the obvious conclusion that the noble gas is not an entirely innocent observer of the isolated fragment but interacts specifically with it, and we must write these species as $M(CO)_5Ng$ (Ng = noble gas). We return later to measurements of this interaction and the theory behind it. The wavelength selective photochemical experiments convert $Cr(CO)_5Xe$ to $Cr(CO)_5Ne$ and *vice versa*, by irradiation in the absorption band of the respective species (we assume that the interaction with Ne is very small).

To unravel more detail of the photochemistry, the use of polarised photolysis and polarised UV/vis/IR spectroscopy proved to be extremely valuable. Because $M(CO)_5$ fragments are not spherically symmetrical, it is possible to select molecules for photolysis according to their orientation, and to examine the orientation of both product and residual reactant molecules.[41,42] The first inference is that the visible band of $M(CO)_5Ng$ species must have the same symmetry as the e vibrational band; this limits the possible excited states for this transition. The second is that the excitation enables $M(CO)_5$ to change from a C_{4v} ground state to a D_{3h} excited state and back again. The energy levels and structures are based on simple MO arguments; see Section 5. We now know what happens in the photochemistry of $M(CO)_6$ in, say Ar. The excited D_{3h} structure of $M(CO)_5$, on collapsing to the C_{4v} structure can do so in three orientations; in one of these, the "vacant site" faces the CO which has just been ejected and recombines with it; in the other two, the site faces an Ar atom and forms $M(CO)_5Ar$ (Fig. 7). This means that the quantum yield should be about 2/3; indeed in solution, the quantum yield was measured[43] to be 0.67. In the reverse reaction, $M(CO)_5 + CO \rightarrow M(CO)_6$, the pentacarbonyl is 'stirred' by absorption in the visible band and reorients until it finds a CO opposite the empty coordination site. In a mixed Ne/Xe matrix, the reorientation enables selective interconversion of $M(CO)_5Xe$ and $M(CO)_5Ne$.

Perhaps the most sophisticated example of unravelling complex photochemistry in a matrix involves $W(CO)_5CS$.[44,45] A combination of wavelength selective photolysis, ^{13}CO isotopic

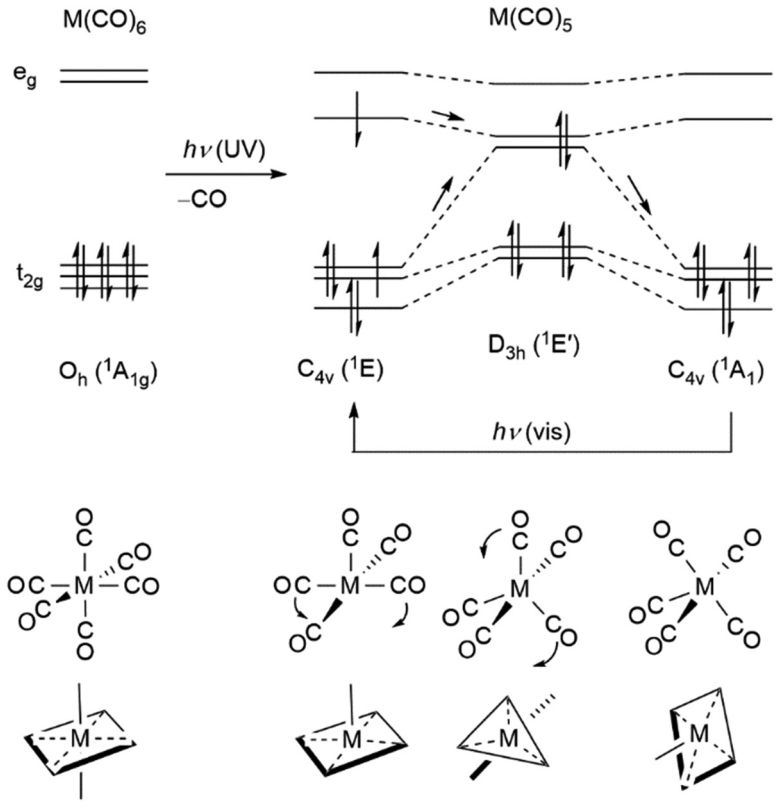

Fig. 7 Orbital energy level scheme, showing the generation of the C_{4v} excited state and its conversion to the C_{4v} ground state *via* the D_{3h} intermediate, so executing a Berry pseudorotation. Adapted with permission from *Inorg. Chem.*, 1978, **17**, 147–154. Copyright 1978, American Chemical Society.[41]

enrichment, including $(^{13}CO)W(CO)_4CS$ labelled specifically *trans* to the CS group, and polarised photolysis and spectroscopy, led to the interpretation shown in Scheme 4. Moreover, it was possible to demonstrate that following loss of CO, the $W(CO)_4CS$ fragment undergoes an excited state rearrangement. The relevance of these experiments to both gas phase and solution metal carbonyl photochemistry will be developed in succeeding sections.

2.1.2 $M(CO)_4$ and $M(CO)_3$ (M = Cr, Mo, W). Prolonged photolysis at short wavelength (< 320 nm) of $M(CO)_6$ molecules in low-temperature matrices leads to the loss of further CO groups.[46] These were identified by following the increase and decrease in C–O band intensities, and also by ^{13}CO substitution. The best data were obtained for the Mo fragments, for which the structures were deduced, and the intensity patterns allowed the estimation of bond angles (Scheme 5). At first sight these structures might be surprising, but, as we shall see, are entirely consistent with simple theory. It should be noted that, as later experiments show, this loss is sequential.

Thus molecules like $W(CO)_5Xe$ or $Cr(CO)_5(CH_4)$ undergo different photochemical processes at different wavelengths. Long-wavelength visible radiation causes ejection of the extra ligand (here Xe or CH_4), while short-wavelength UV radiation causes loss of CO to form a tetracarbonyl. Wavelength-dependent photochemistry is a critical characteristic.

Matrix isolation can answer an additional question about these reaction intermediates. The metal hexacarbonyls are air stable in the absence of UV irradiation, but why do they decompose rapidly in the presence of air and UV radiation

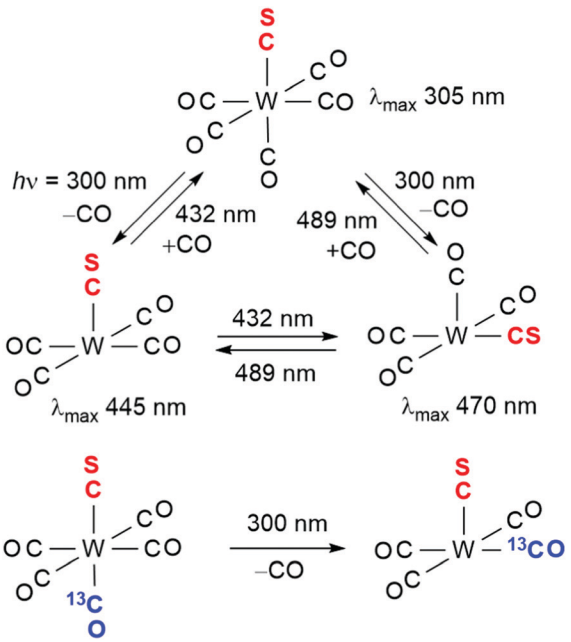

Scheme 4 Photochemistry of $W(CO)_5(CS)$ in an argon matrix, adapted with permission from *Inorg Chem.*, 1976, **15**, 2892–2897. Copyright 1976, American Chemical Society.[45]

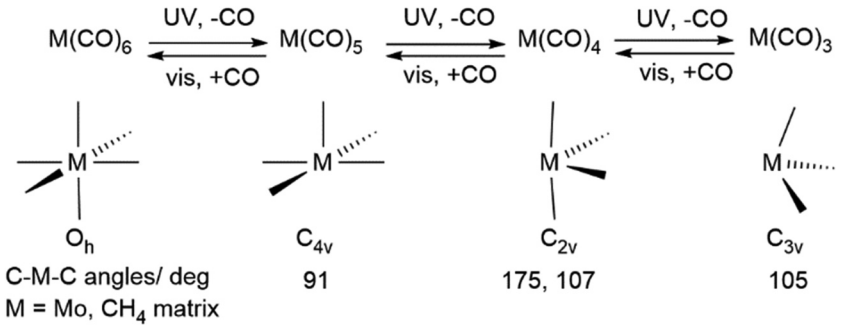

Scheme 5 Sequential CO photodissociation of $M(CO)_6$ (M = Cr, Mo, W) in matrices and structures of photofragments.

forming metal oxides? The intermediates that are formed have been identified by photolysis in O_2-doped matrices to be oxo species $M(O)_2(CO)_4$, $M(O)_2(CO)_2$ and peroxo species such as $(\eta^2\text{-}O_2)M(CO)_x$ (x = 3 or 4), prior to forming molecular oxides MO_2 (M = Cr, Mo) and MO_3 (M = Mo, W).[47]

2.1.3. Co-condensation of metal atoms with CO. There is another way of producing unstable species in a matrix: co-condensation of reactive partners. For metal carbonyls this technique was exploited by Ozin, but more particularly by Andrews.[48] In his method, laser ablation of a metal surface generates a stream of metal atoms, which are co-condensed with CO and an excess of a noble gas onto a cold, IR-transparent window. Fragments are identified by the spectroscopic changes on matrix warming, photolysis, and by isotopic enrichment. Where there is overlap between the methods of photolysis of a stable precursor and the co-condensation methods, the agreement is very good.

In a recent interesting exploitation of this technique in combination with photochemistry, Wu *et al.*[49] co-condensed a stream of laser-ablated Ca, Sr or Ba atoms with Ne doped with CO. The IR spectra showed, in each case, a single CO band, assigned *via* isotopic enrichment, to an $M(CO)_8$ species. The strong back-bonding produced substantial shifts in the C–O frequencies. At lower concentrations of CO, $M(CO)_n$ (n = 2, 3, 4) were formed; their bands were distinguished from one another by their photochemical response.

2.2 Photochemistry of $Fe(CO)_5$ and $CpMn(CO)_3$

2.2.1 $Fe(CO)_4$ and $Fe(CO)_3$. The photochemistry of $Fe(CO)_5$ in low temperature matrices is somewhat complex,[50–54] but its behaviour is vital to the understanding of the photochemistry in gas phase and solution (Scheme 6). As mentioned above, there is no evidence of crossing from a singlet (spin-paired)

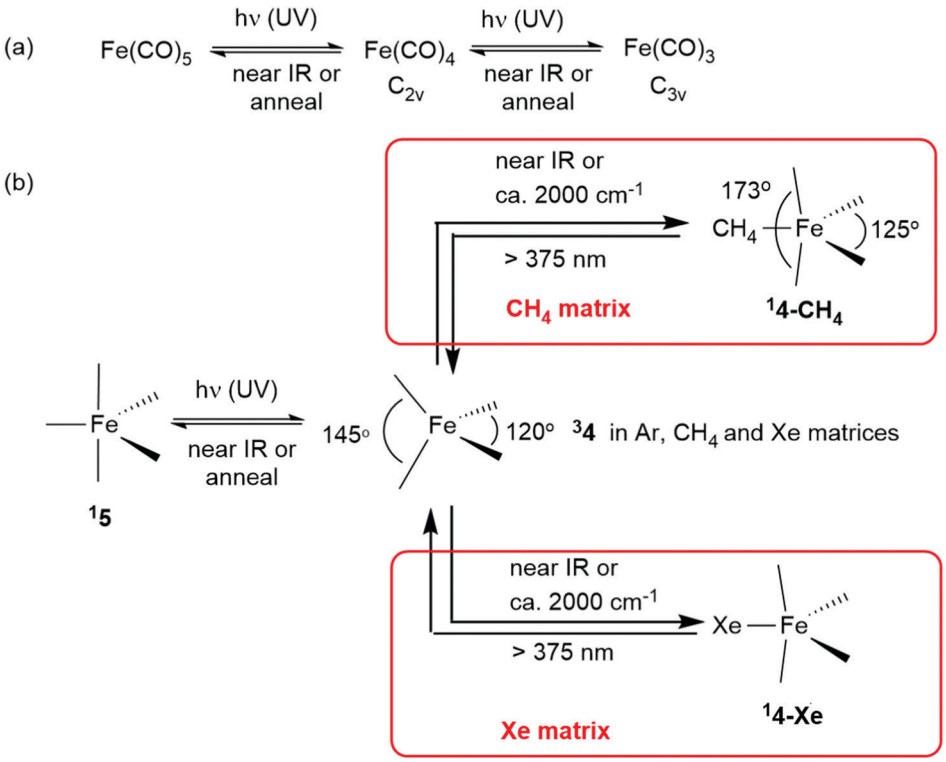

Scheme 6 (a) Photochemistry of $Fe(CO)_5$ in matrices. (b) Formation and structures of $Fe(CO)_4$ and its adducts. For notation, see text.

manifold to a triplet (spin parallel) manifold prior to ejection of CO in any of the binary metal carbonyls. However, this does not preclude a spin-state change after ejection of CO. Indeed, $Fe(CO)_5$ follows this course of events and $Fe(CO)_4$ is generated in its triplet state (^{3}**4**) as proved by magnetic circular dichroism experiments.[53] In Xe and CH_4 matrices, there is considerable, reversible, reaction to produce singlet species (^{1}**4-Xe** and ^{1}**4-CH$_4$**) with structures different from that of ^{3}**4**; there was no evidence for "uncomplexed" ^{1}**4**. It is noteworthy that in a hydrocarbon glass at 77 K, only the species ^{1}**4-alkane** was produced. In neither Ne or Ar matrices was there any production of singlet states such as ^{1}**4-Ne** or ^{1}**4-Ar**, only reversal to the parent molecule. We take up the important story of spin states later. Unlike the different $Cr(CO)_5Ng$ species, ^{3}**4** could be distinguished from ^{1}**4-Xe** by IR spectra because of the different geometries of ^{3}**4** and ^{1}**4-Xe**. Again, the structures of these species are, at first sight, surprising, but were later rationalised by theory (Section 5). Moreover, as we shall see in the Gas Phase section, the behaviour is entirely consistent with elegant gas-phase electron diffraction measurements[55,56] on $Fe(CO)_4$.

Prolonged short wavelength photolysis of $Fe(CO)_5$ in a low-temperature matrix generates the C_{3v} fragment $Fe(CO)_3$ with C–O bands at 2040.1 (a_1) and 1930.4 (e) cm^{-1} in a CH_4 matrix, and 2042/1935.6 cm^{-1} in an Ar matrix. From the relative intensities of the two bands, a C–Fe–C bond angle of 108 ± 3° was estimated.[57] Thus $Fe(CO)_4$ also exhibits wavelength-dependent photochemistry. Importantly, Burdett (see Theory section) calculated a bond angle of 111°, which demonstrates that the deviation from a naively expected trigonal D_{3h} structure is real and not due to interaction with the matrix.

2.2.2 Photochemistry of CpMn(CO)$_3$. Although early studies showed that photolysis of $CpMn(CO)_3$ in matrices generates $CpMn(CO)_2$, only part of the story was revealed at that stage. Following evidence from solution studies (Section 4), McMahon and colleagues[58] have probed deeper into the matrix photochemistry of $CpMn(CO)_3$. In experiments reminiscent of the early $Fe(CO)_4$ studies, they showed that UV photolysis generates a mixture of singlet and triplet $CpMn(CO)_2$ as had been proposed in solution (Section 4.4.3), the latter with a remarkably large separation between the two ν(CO) bands. By long wavelength irradiation of $CpMn(CO)_2(C_2H_4)$, they could generate singlet $CpMn(CO)_2$ selectively; irradiation with >300 nm converted ^{1}[$CpMn(CO)_2$] to the triplet form which reverted slowly, even in the dark at 10 K, to the singlet state. DFT calculations reproduce the enlarged separation of the ν(CO) bands quite well with a pyramidal structure for the triplet state.

2.3 Photochemistry of Mn$_2$(CO)$_{10}$, HMn(CO)$_5$ and [CpFe(CO)$_2$]$_2$

2.3.1 Mn$_2$(CO)$_9$ and Mn(CO)$_5$. Conventional UV/Vis flash photolysis of $Mn_2(CO)_{10}$ studies[59] in solution suggested that there were two photolysis products, the radical $Mn(CO)_5$ and the CO-loss species $Mn_2(CO)_9$, but without structural characterisation it was not possible to be certain of the assignment. By photolysing $Mn_2(CO)_{10}$ in a hydrocarbon glass at 77 K, Hepp and Wrighton were able to prove that there was CO loss and the formation of a species with a single bridging CO group.[60] Warming the glass allowed the recombination of CO and bridged species to the parent. Later, in an ingenious experiment in Ar at 12 K, Dunkin *et al.* employed polarised photochemistry and spectroscopy to show that the CO vector of the bridging group lay at *ca.* 45° to the Mn–Mn axis, consistent with the low value of ν(CO) 1764 cm^{-1} (Scheme 7).[61]

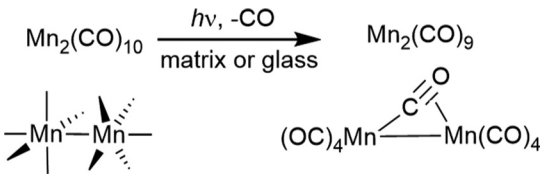

Scheme 7 Photochemistry of $Mn_2(CO)_{10}$ in matrices and glasses.

In neither case was there any evidence for $Mn(CO)_5$.The reason is that any splitting of the Mn–Mn bond produces two radicals sitting next to each other, and they are too big to escape the surrounding glass/matrix cage, so they simply recombine. To establish the existence of $Mn(CO)_5$ and determine its structure a slightly roundabout method is required.

Photolysis of $HMn(CO)_5$ in a CO matrix leads to two processes: the major one is loss of CO to produce $HMn(CO)_4$ (see above). In the minor process, loss of H occurs to produce $Mn(CO)_5$ plus HCO. Because the $HMn(CO)_4$ is sitting in a sea of CO, it readily recombines to form the parent, allowing the spectrum of $Mn(CO)_5$ to be monitored. A combination of ^{13}CO isotopic enrichment, polarised photolysis/spectroscopy, and intensity measurements confirmed that the product is indeed $Mn(CO)_5$ with a C_{4v} structure and an axial-equatorial angle of about 96°.[62] EPR spectra following gamma-irradiation of $HMn(CO)_5$ in krypton at 77 K, demonstrates the generation of $Mn(CO)_5Kr$, (*i.e.* a species reminiscent of the $M(CO)_5Ng$ systems described earlier) and confirmed its C_{4v} structure (Scheme 8).[63]

2.3.2 [CpFe(μ-CO)$_3$FeCp]. As shown above, glass work did not become redundant with the development of noble gas matrices. Mark Wrighton, in particular, made extensive use of glasses to unravel some fascinating photochemistry. Tony Rest pioneered the application of polymer films at low temperature. We give an example of where their work overlapped.[64,65] In similar vein to the studies on $Mn_2(CO)_{10}$, solution experiments on the photochemistry of $[CpFe(CO)_2]_2$ showed that two species were produced. In the glass and matrix/polymer studies, it was proved, by elegant ^{13}CO substitution, that on UV irradiation of parent, the symmetrical triply-bridged species $[CpFe(\mu\text{-}CO)_3FeCp]$ (Ar: single ν(CO) at 1812 cm^{-1}) was generated. Indirect confirmation of this conclusion was the photolytic production of

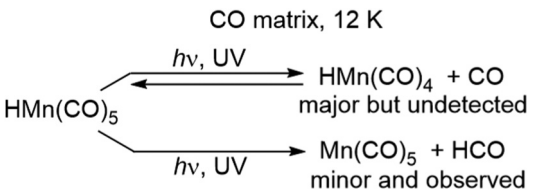

Scheme 8 Photochemistry of $HMn(CO)_5$ in CO matrices.

the symmetrical triply-bridged $[(\eta^5\text{-}C_5Me_5)Fe(\mu\text{-}CO)_3(\eta^5\text{-}C_5Me_5)]$, which was stable enough to permit proof of its D_{3h} structure by X-ray diffraction and determination of its magnetic moment corresponding to a triplet ground state.[66]

Once more, none of the proposed radical photoproduct, $CpFe(CO)_2$, was identified in the matrix studies because of the cage effect. However, in an experiment significant for solution studies, (see later) it was demonstrated that prolonged photolysis of $[CpFe(CO)_2]_2$ in a 3-methylpentane glass at 98 K, yielded $[CpFe(CO)]_2$, (ν(CO) = 1958 and 1904 cm^{-1}; *i.e.* with no bridging CO group) presumably *via* photolysis of the triply bridged species.[67]

Matrix photochemistry: key points
(1) Matrix isolation (10–20 K) in solid Ne, Ar, Kr, Xe or CH_4 to observe ν(CO) IR bands of primary products of photodissociation. Product accumulates over time during irradiation and remains stable at conditions of measurement.
(2) Alternatively, use hydrocarbon glasses, but less inert (77 K).
(3) Coordinatively unsaturated metal carbonyls exhibit long-wavelength UV/vis absorption.
(4) Reversibility of photodissociation on irradiation into this long-wavelength absorption.
(5) Isotopes and energy-factored force fields (EFFF) to determine geometry of products of loss of one or two CO groups (*e.g.* $Cr(CO)_5$, $Fe(CO)_4$, $Fe(CO)_3$).
(6) OC–M–CO bond angles estimated from intensity ratios of ν(CO) IR bands.
(7) Interaction of $M(CO)_5$ (M = Cr, Mo, W) and $Fe(CO)_4$ with Xe and CH_4.
(8) Wavelength selective photochemistry: recombination with CO *vs.* loss of further COs.
(9) Cage effect prevents observation of M–M bond cleavage in the matrix.
(10) Polarised photochemistry to probe photochemical mechanism.
(11) Use of magnetic circular dichroism for evidence of paramagnetism of $Fe(CO)_4$.

3. Photochemistry in the gas phase

3.1 Formation of multiple fragments on single photon absorption

3.1.1 $Fe(CO)_x$ fragments. In 1981, Yardley and colleagues described experiments in which mixtures of $Fe(CO)_5$ and PF_3 were subjected to pulsed laser irradiation, at different wavelengths, and the products analysed by gas chromatography.[68] An analysis of the yields of $Fe(CO)_x(PF_3)_{5-x}$ (Table 2) was consistent with single photon absorption producing $Fe(CO)_x$ fragments; the higher the laser energy, the greater the number of CO groups that were lost. The reason is that the photoproducts are generated in vibrationally and electronically excited states that cannot dissipate their excess energy without collisions. The photofragments are generated sequentially in a process like a firework that ejects flares in rapid succession. Similar behaviour has been reported for group 6 hexacarbonyls. This contrasts with practically all experiments in condensed phases where only a single CO is lost on pulse irradiation. We shall return to the theory behind this shortly.

It will be evident from the identification of carbonyl fragments in low-temperature matrices by IR spectroscopy, that the undisputed identification of fragments in the gas phase would also benefit from IR spectroscopy. The problem, of course, is timescale; such fragments in the gas phase are expected to be very short-lived. Eric Weitz and colleagues were the first to tackle this problem.[69] Various gas mixtures of $Fe(CO)_5$/Ar/CO were photolysed with a pulsed KrF excimer laser (248 nm) and the change in IR transmitted intensity monitored at a series of different wavelengths with a CO laser. The identification of the $Fe(CO)_x$ fragments follows directly from the species identified in matrices,[50] with slight shifts from matrix to gas of about 10 cm^{-1} (Fig. 8). It is important to note that at this gas pressure and over this timescale of several μs, the fragments are observed in their triplet ground states. The rate of recombination of $Fe(CO)_4$ with added CO was $(3.5 \pm 0.9) \times 10^{10}$ dm^3 mol^{-1} s^{-1}. A further feature of these gas phase spectra is that the band centres shift slightly to shorter wavelengths with time. As explained later, this shift is due to relaxation of 'hot' molecules.

Table 2 Dependence of relative yields of $Fe(CO)_5$ photofragments on laser wavelength/energy (dominant fragment shown in bold font)

Photolysis laser	Nd:YAG	KrF	ArF
Wavelength/nm	355	248	193
Photon energy/kcal mol^{-1}	80.5	115.3	148.1
Photofragment	**Relative yields**		
Fe(CO)			0.012
$Fe(CO)_2$	0.31	**0.55**	**0.81**
$Fe(CO)_3$	**0.46**	0.35	0.09
$Fe(CO)_4$	0.23	0.10	0.09

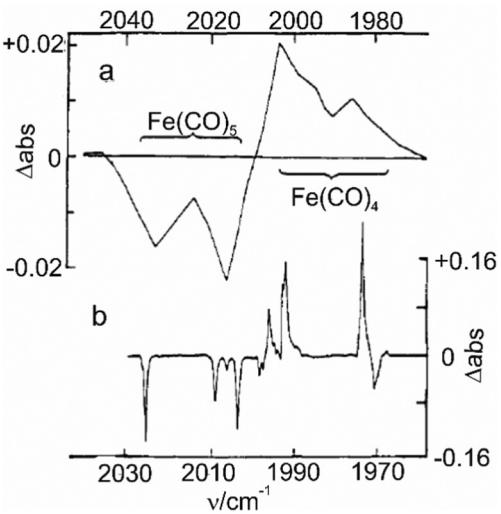

Fig. 8 Comparison of IR difference spectra for $Fe(CO)_5$ and $Fe(CO)_4$ in gas phase with those in argon matrix. The bands of $Fe(CO)_5$ appear negative whereas those of $Fe(CO)_4$ appear positive. (a) TRIR spectra 3 μs after laser pump flash of $Fe(CO)_5$ in the gas phase in presence of 100 torr CO; (b) FTIR spectra after photolysis of $Fe(CO)_5$ in Ar matrix at 10 K. To aid comparison the wavenumber scales have been shifted 10 cm^{-1} relative to each other to compensate for the solvent effect of argon. Adapted with permission from *Acc. Chem. Res.*, 1987, **20**, 408–414. Copyright 1987, American Chemical Society.[54]

Weitz also observed that the gas phase IR spectra of the carbonyl fragments were very broad. How to overcome this? As explained by Tanaka *et al.*,[70] vibrational cooling in supersonic jet expansion produces very narrow lines, for example, of the fragments Fe(CO) and $Fe(CO)_2$, produced in their triplet ground states ($^3\Sigma^-$ and $^3\Sigma_g^+$, respectively) by ArF (193 nm) and KrF (248 nm) laser photolysis of $Fe(CO)_5$. This method generated very high-resolution spectra and accurate rotational constants, leading to moments of inertia.

3.1.2 $M(CO)_x$ fragments (M = Cr, Mo, W). In important experiments, Wells and Weitz examined the TRIR spectra following laser flash of $M(CO)_6$ (M = Cr, Mo, W) with Xe, Kr and Ar.[71] Based on the matrix work,[40] they were able to identify $M(CO)_5Xe$ species and $W(CO)_5Kr$. By monitoring the kinetics of recovery to $M(CO)_6$, they obtained recombination rates ($Cr(CO)_5$ + CO; $(1.5 \pm 0.3) \times 10^{13}$ dm^3 mol^{-1} s^{-1}), estimated the dissociation energies for the Xe complexes and placed an upper limit on the dissociation energies of Kr–$W(CO)_5$ and Ar–$W(CO)_5$. We shall return to these numbers in Section 4.3.

3.1.3 $Mn_2(CO)_9$ and $Mn(CO)_5$. Weitz and coworkers also looked at $Mn_2(CO)_{10}$ in the gas phase.[72] On the basis of matrix data (see above) and solution data (Section 4.2), they were able to detect both $Mn(CO)_5$ and $Mn_2(CO)_9$, and monitor their kinetics. Not surprisingly the relative yield of $Mn_2(CO)_9$ to $Mn(CO)_5$ increased with increasing laser frequency.

Studies by Weitz and colleagues,[71] and by the groups of Rosenfeld and Rayner/Hackett allowed, largely on the basis of matrix IR data, the identification of a whole slew of metal carbonyl fragments, and determination of their reaction kinetics.

3.2 Alternative techniques for gas-phase photochemistry

3.2.1 Electron diffraction. Of the results with different methods, unquestionably the most impressive have been the electron diffraction experiments by Zewail and colleagues.[55,56] Following a fs UV laser pulse on $Fe(CO)_5$, it was possible to record and simulate the diffraction patterns, allowing determination of the structure of $Fe(CO)_4$. There were two important conclusions: over the detection lifetime, the species was in the singlet state; its structure was very similar to that determined for $^1[Fe(CO)_4–CH_4]$ in the matrix experiments (Section 2). The connection between these two sets of widely different techniques has been outlined by Poliakoff and Turner.[52] The singlet state is observed because, over the lifetime of the electron diffraction measurement, the singlet state has not time to relax to the triplet ground state. The bond angles calculated for $Fe(CO)_4$ from these sophisticated electron diffraction measurements were almost identical to those estimated from non-digitized IR spectra from the matrix integrated by literally cutting out the peaks from the chart paper and weighing!

3.2.2 Mass spectrometry and cryogenic ion vibrational spectroscopy. Mass spectrometry is also a powerful method for detection of metal carbonyls following UV laser photolysis of metal carbonyls. In Section 5 on Theory and gas-phase dynamics, we will consider the experiments by Fuss and colleagues and their significance. However, given the increasing interest in photoCORMs (see Introduction), we exemplify a very recent sophisticated experiment.[73] Attempts to correlate the behaviour of photoCORMS with theory (mostly DFT) is complicated by the necessity to account for solvent effects on the photochemistry. Thus gas phase experiments would provide useful data. TryptoCORM $[MnL(CO)_3(CH_3CN)]$; (L = deprotonated Tryptophan) was electrosprayed to produce the gas phase ions, $[MnL(CO)_3(CH_3CN)]\cdot H^+$, and $[MnL(CO)_3]\cdot H^+$. These ions were examined by the novel technique of cryogenic ion vibrational spectroscopy.[74] In this method, following electrospraying, gas phase ions, such as $MnL(CO)_3\cdot H^+$, are collected at 10 K in a 3D quadrupole ion trap, and then "tagged" with a loosely-bound non-interacting species, X_n, such as a rare gas or H_2/D_2, to produce $[MnL(CO)_3\cdot H^+]\cdot X_n$, with various n. A mass spectrometer is used to select one of these species, say $n = n'$. The interaction energy between $X_{n'}$ and the rest of the complex is very weak, in the range of vibrational frequencies. Thus irradiation with an IR laser at one of the vibrational frequencies of the complex is followed by energy redistribution, which results in $X_{n'}$ being ejected, whereby the resulting $MnL(CO)_3\cdot H^+$ ion can be detected in a mass spectrometer. The IR laser frequency is then scanned to the next absorption. Thus the very low temperature IR spectrum of the complex can be obtained.

In addition, UV/vis absorption spectra of $MnL(CO)_3\cdot H^+$ and $MnL(CH_3CN)(CO)_3\cdot H^+$ were obtained by photodepletion of mass-selected ions with a tunable pulsed laser and the formation of photofragments was recorded as a function of excitation wavelength. These experiments reveal very strong dependence of the photofragmentation patterns of $MnL(CO)_3(CH_3CN)\cdot H^+$ on the excitation wavelength with CH_3CN lost at the lowest photon energies, three CO groups lost at intermediate energies and both CH_3CN and 3COs at the highest photon energies.[73] In contrast to the gas phase, only one CO is lost from $MnL(CO)_3(CH_3CN)$ in solution.[75]

3.2.3 Photoelectron spectroscopy. A very recent interesting development combines laser photolysis with time-resolved valence and core-level photoelectron spectroscopy.[76,77] In these experiments, following a 266 nm laser flash (140 fs) on $Fe(CO)_5$, the generated fragments are probed with an X-ray pulse (100 fs) from a free-electron laser. Signals are interpreted on the basis of sophisticated theoretical calculations, and assigned to $Fe(CO)_5$, $Fe(CO)_4$ and $Fe(CO)_3$, confirming that the species are generated in singlet states, with no evidence for the ground triplet states before 6 ps, exactly as expected. It is supposed that conversion to the triplet states requires collisional relaxation. The experiments also demonstrate that the photofragments are generated sequentially, first $Fe(CO)_4$ and then conversion to $Fe(CO)_3$ with time constant of 3 ps. The first valence ionization energy of $Fe(CO)_4$ is reduced by 0.7 eV compared with $Fe(CO)_5$, whereas the core 3σ orbital of bound CO increases in ionization energy by *ca.* 2–3 eV.

Gas phase photochemistry: key points

(1) Dissociation of multiple CO molecules on absorption of a single UV/vis photon.
(2) Number of CO groups ejected increases with photon energy.
(3) Measurements of kinetics of reaction of photoproducts with CO and other ligands.
(4) Estimation of Ng–$M(CO)_5$ (M = Cr, Mo, W) bond energies.
(5) Photofragmentation patterns by mass spectrometry.
(6) Time-resolved electron diffraction and photoelectron spectra of photofragments.

4. Photochemistry in solution

4.1 Time-resolved UV/visible and infrared (TRIR) spectroscopy of $M(CO)_6$ (M = Cr, Mo, W)

Can the initial products of photolysis be detected in solution? We start with a simple early experiment.[78] Conventional UV/vis flash photolysis of $Cr(CO)_6$ in cyclohexane, with a time resolution of about 3 μs, demonstrated the appearance of a transient with an absorption maximum at 503 nm. In a solution saturated under an atmosphere of CO, this transient regenerated $Cr(CO)_6$ with a half-life of 25 μs. In a methane matrix (see above), $Cr(CO)_5(CH_4)$ has a band at 489 nm. Given that both media involve saturated hydrocarbons it is reasonable to assign the solution transient to $Cr(CO)_5$(cyclohexane).

More evidence came from the first time-resolved IR experiments, also carried out by the Mülheim group.[79] With very simple equipment, and employing the same conditions as in the UV/vis experiments, they detected a species with an IR band at 1962 cm^{-1} matching the most intense band of $Cr(CO)_5(CH_4)$ in the methane matrix that appears at 1961 cm^{-1}. It seemed reasonable to assign the band to $Cr(CO)_5$(cyclohexane). The assignment was confirmed by irradiation of $Cr(^{12}CO)_5(^{13}CO)$ and analysis of the product bands due to $Cr(^{12}CO)_5$(cyclohexane) and $Cr(CO)_4(^{13}CO)$(cyclohexane) isotopologues.

In another significant early experiment, Bonneau and Kelly,[80] again *via* conventional UV/vis flash photolysis, examined the behaviour of $Cr(CO)_6$ in perfluoromethylcyclohexane solvent. They reasoned that the matrix data[40] on $Cr(CO)_5L$ suggested that the interaction of $Cr(CO)_5$ with the perfluoro solvent would be weaker than with cyclohexane (matrix data λ_{max} $Cr(CO)_5(CF_4)$ 547 nm compared with $Cr(CO)_5(CH_4)$ 489 nm). The flash yielded a short-lived intermediate (half life ~38 ns in CO-saturated solution), with an absorption centred at 620 nm, close to that of $Cr(CO)_5Ne$ at 624 nm. Both of these observations argue for the reactions in eqn (6) occurring in solution:

$$Cr(CO)_6 \xrightarrow{h\nu,-CO} Cr(CO)_5 \xrightarrow{L} Cr(CO)_5L \xrightarrow{+CO,-L} Cr(CO)_6 \quad (6)$$

"Naked" $Cr(CO)_5$ was too short-lived to be detected (but see below). The reaction with CO is faster in the more weakly bound perfluoro solvent. Photochemistry in perfluoro solvents continues to play an important part in mechanistic studies, and we return to these solvents several more times.

The thermal displacement of cyclohexane in $Cr(CO)_5$-(cyclohexane) by heterocyclic ligands has also been followed by TRIR. The reactions occur by associative or interchange mechanisms with rates that are dependent on the entering ligand. For example, reaction with THF occurs within 10 μs at 0.02 M THF. These studies[81] are important for understanding the mechanism of typical synthetic procedures for photochemical substitution that continue to be popular. Related studies[82] have reported time-resolved absorption measurements to monitor the conversion of $Cr(CO)_5(\eta^2$-benzene) to $Cr(CO)_5$(THF). These experiments, usually (but see later) show the loss of only one CO group. The accepted reason is that the 'hot' $Cr(CO)_5$ rapidly loses excess energy to the surrounding solvent bath before any further CO groups are lost, in contrast to the gas phase behaviour, where multiple CO loss can occur.

In the time-resolved experiments described so far, the species detected is $Cr(CO)_5$(solvent), not 'naked' $Cr(CO)_5$; can the naked species be detected? Any attempt will involve much faster technology. On a very fast timescale with UV/vis detection, it was concluded[83] that the dissociation of a CO group occurs within 300 fs and complexation to the solvent is complete within about 1 ps. This short timescale for dissociation reflects the studies in the gas phase.

There is a further complication. As mentioned in the gas phase studies, the C–O vibrational spectrum shifts slightly with delay time. What happens in solution? This is illustrated in elegant experiments by Dougherty and Heilweil.[84] Fig. 9 shows the TRIR spectra following laser photolysis of $W(CO)_6$ in *n*-hexane. At the longest timescale (333 ps), the spectrum shows depletion of $W(CO)_6$ at 1983 cm^{-1}, and the formation of two bands at 1956 and 1928 cm^{-1}. Comparing these to the bands in a CH_4 matrix [$W(CO)_6$, 1982 (t_{1u}); $W(CO)_5$, 1957 (e), 1926 (a_1)] clearly establishes this species as $W(CO)_5$(*n*-hexane). At 73.3 ps, there are two other bands in the spectrum at 1942 and 1908 cm^{-1} which disappear at the same rate and are thus assigned to the same species. The decay time is 160 ± 20 ps, which is reminiscent of the decay time for the $v = 1$ to $v = 0$ decay

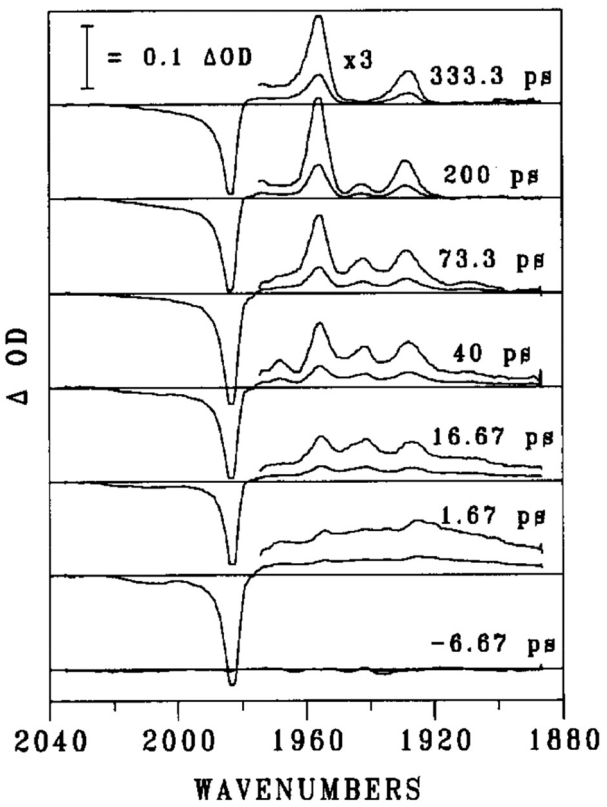

Fig. 9 Transient IR difference spectra for $W(CO)_6$ in *n*-hexane following UV excitation. Reprinted from *Chem. Phys. Lett.*, 1994, T. P. Dougherty and E. J. Heilweil, "Ultrafast transient infrared absorption studies of $M(CO)_6$ (M = Cr, Mo or W) photoproducts in *n*-hexane solution", **227**, 19–25, Copyright 1994, with permission from Elsevier.[84]

time of the t_{1u} mode of $W(CO)_6$ (140 ± 15 ps) in hexane established by IR pump-probe experiments. The −14 cm^{-1} shift of the e band of $W(CO)_5$ (*n*-hexane) from 1956 to 1942 cm^{-1} similarly matches the −15 cm^{-1} from the fundamental $v = 0 \rightarrow v = 1$ to the $v = 1 \rightarrow v = 2$ mode of $W(CO)_6$ corresponding to the anharmonicity.[85] This strongly suggests that we are looking at the decay of vibrationally excited ($v = 1$) $W(CO)_5$(*n*-hexane). The bands at 1942 and 1908 cm^{-1} are fully consistent with the vibrationally excited species, yielding anharmonic shifts of −14 and −20 cm^{-1}. At the shortest timescale (1.67 ps), there is a hint of these four bands, but they are broadened almost beyond recognition. This broadening arises because of the coupling of the C–O stretches to lower vibrational modes which are in high vibrational states. Over some 40 ps, these vibrational modes relax to their ground states and the broadening vanishes. The importance of this broadening will depend on the system, and the shorter the wavelength of the photolysis laser, the more energy dumped in the fragment, and the greater the problem, as happens in the gas phase. This clearly makes assignment at very short times extremely difficult.

Harris and colleagues have probed the photochemistry of the $M(CO)_6$ (M = Cr, Mo, W) species on the even faster fs timescale.[86] Not surprisingly, the analysis is complicated by the band broadening, but, in addition, coherent oscillations arising from the pump and probe pulses (free induction decay) present a problem. Nonetheless, they were able to conclude that hot $Cr(CO)_5$ molecules react with ejected CO molecules which have not escaped the solvent cage in <300 fs. This geminate recombination is the analogue of the cage effect in matrices. The band broadening is also associated with the dynamics of rearrangement of the solvent coordination as is illustrated by a study of the $Cr(CO)_6$ in alcohol solvents. The $Cr(CO)_5$ moves along the alkyl chain of the solvent until it eventually coordinates to the hydroxyl group. The time constants for these processes vary according to the alkyl chain and range from *ca.* 200 to 2000 ps.[87]

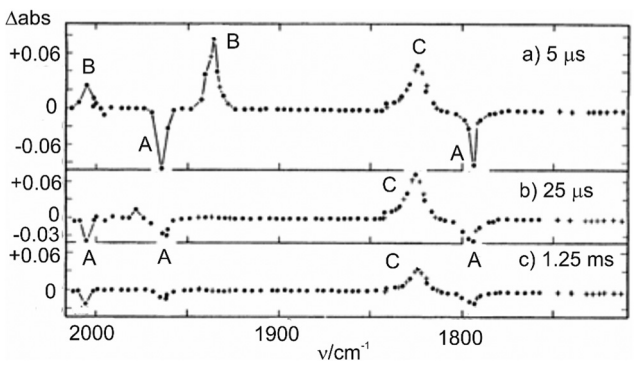

Fig. 10 Transient difference spectra showing change in absorbance: (a) 5 μs, (b) 25 μs, and (c) 1.25 ms after the UV flash photolysis of $[CpFe(CO)_2]_2$ in cyclohexane solution under 1 atm pressure of CO. A = $[CpFe(CO)_2]_2$, B = $CpFe(CO)_2$, C = $CpFe(\mu\text{-}CO)_3FeCp$. Reproduced from ref. 90 with permission from the Royal Society of Chemistry.

4.2 Photochemistry of $Mn_2(CO)_{10}$ and $[CpFe(CO)_2]_2$

4.2.1 $Mn_2(CO)_{10}$. Following their success with $Cr(CO)_5$(cyclohexane), the Mülheim group[88] looked at $Mn_2(CO)_{10}$, building on earlier conventional UV/vis flash photolysis experiments – which established that there must be two photochemical pathways – and matrix isolation data. They detected $Mn(CO)_5$, assuming that the IR band observed at 1990 cm^{-1} was due to the unresolved a_1 and e bands established in the CO matrix (1978.4 and 1987.6 cm^{-1}).[62] In addition, several bands due to $Mn_2(CO)_9$ were detected, in particular the band at 1760 cm^{-1}, due to the semibridging CO group described earlier (Scheme 7).[61] They were able to measure the recombination rate of the $Mn(CO)_5$ radicals ($k \sim 10^9$ dm^3 mol^{-1} s^{-1}) and the rate of reaction of $Mn_2(CO)_9$ with CO ($k \sim 10^6$ dm^3 mol^{-1} s^{-1}). The semibridging species, $(CO)_4Mn(\mu\text{-}CO)Mn(CO)_4$ is unlikely to be a primary product, since the starting species has no bridging CO, and hence the primary act is probably loss of a terminal CO to produce $(CO)_5MnMn(CO)_4$ (see Section 5.4 for the wavelength dependence and theory of the photochemistry).[89] The elucidation of the photochemistry of $Mn_2(CO)_{10}$ and related dinuclear complexes relates directly to the studies of photopolymerisation (Section 1.1).[11]

4.2.2 $[CpFe(CO)_2]_2$. Another dimeric species that has been studied extensively is $[CpFe(CO)_2]_2$, which has two bridging CO groups (*i.e.* $Cp(CO)Fe(\mu\text{-}CO)_2Fe(CO)Cp$), and which exists in both *cis* and *trans* forms. Based on the matrix/glass data (Section 2.3), two species were identified conclusively by TRIR, the CO-loss product $CpFe(\mu\text{-}CO)_3FeCp$ and the radical $CpFe(CO)_2$ (Fig. 10).[90] The radical (labelled B in Fig. 10) dimerises quickly to reform the precursor (A) while the triply-bridged species (C) reacts with CO much more slowly also to reform A (Scheme 9).

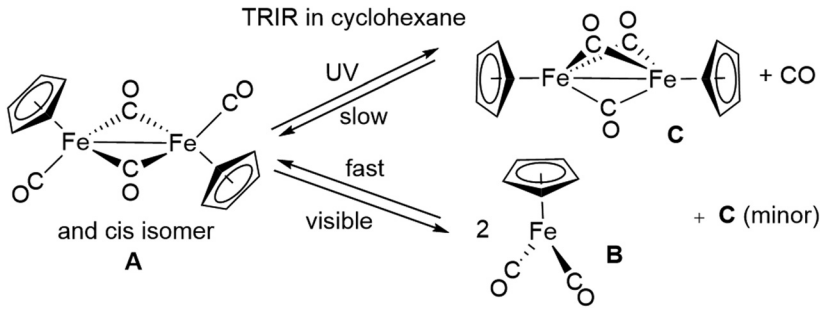

Scheme 9 TRIR photochemistry of $[CpFe(CO)_2)]_2$ in cyclohexane under CO.

Since this study, there have since been many investigations[91] of the photochemistry of $[CpFe(CO)_2]_2$, over the time range ps to fs. Everyone agrees that on visible photolysis the initial product, generated in about 2 ps, is the radical $CpFe(CO)_2$, and its subsequent reactions have been followed. UV photolysis produces some radical, and the triply-bridged $[CpFe(\mu\text{-}CO)_3FeCp]$. The majority of the $[CpFe(\mu\text{-}CO)_3FeCp]$ is generated with time constant *ca.* 20 ps and decays over a relatively long time by reaction with, for example, MeCN[92] or alkenes,[93] to yield $Cp(CO)Fe(\mu\text{-}CO)_2FeCp(L)$.

Although the radical is an obvious primary product, the same cannot be said for the triply-bridged species, and there have been many attempts to determine the primary step. The most recent effort[91] suggests that one path with time constant 23 ps involves the expected $[Cp(CO)Fe(\mu\text{-}CO)_2FeCp]$, formed by loss of a terminal CO but this intermediate has never been identified. The other route, providing *ca.* 16% of $[CpFe(\mu\text{-}CO)_3FeCp]$ is more intriguing since it involves the one-photon loss of two CO groups, a very unusual event, but not unique. The assignment of this species relied on the study in glasses,[67] and postulates that this species reacts with CO with time constant *ca.* 45 ns to form $[CpFe(\mu\text{-}CO)_3FeCp]$.

4.3 Use of liquefied and supercritical noble gases

The use of liquefied noble gases (see Section 1.2) provided an opportunity for looking at the interaction between $M(CO)_5$ fragments and noble gases. In the first experiment we were able to detect by FTIR, the species $Cr(CO)_5Xe$, generated by photolysis of $Cr(CO)_6$ in liquid Xe at −98 °C, with C–O bands almost identical to those in a solid Xe matrix, and with a lifetime of about 2 s.[94] In an important development, Weiller[95] repeated this experiment and in addition, by using rapid scan FTIR, monitored the kinetic behaviour of the species $M(CO)_5Ng$ (M = Cr, W; Ng = Xe, Kr) for reaction with CO over the temperature range 173 to 198 K. In this way he was able to obtain a minimum value‡ for the Xe–$W(CO)_5$ bond dissociation of 8.4 ± 0.2 kcal mol^{-1}, in remarkable agreement with Weitz's gas phase value.

These experiments were conducted well below room temperatures, but even so required fairly high pressure cells. To conduct such experiments near room temperature, in the region where such solvents become supercritical (sc), requires apparatus operating at much higher pressures. George and colleagues[96] studied the interaction between photochemically generated $M(CO)_5$ species (M = Cr, Mo, W) and the solvents Xe and Kr at or above room temperature. Combining laser irradiation and IR diode laser detection, they obtained a value of 8.2 ± 0.2 kcal mol^{-1} for the Xe–W interaction. The Cr and Mo analogues reacted considerably faster, indicating lower Xe–M bond energies, in contrast to the numbers obtained by Weitz (Table 3). We shall come back to this point in due course. Of equal importance, by both TRIR and UV/vis detection, there was intriguing evidence in these room temperature solutions of interaction with Ar, although it was not possible to obtain any definitive assignment or bond energy numbers. To reduce carbonyl fragment-noble gas interactions further, one needs liquid Ne, corresponding to the Ne matrix experiments, but as far as we are aware, no one has attempted this.

‡ If the substitution mechanism is dissociative, the enthalpy of activation for substitution by CO can be equated to the bond energy. If there is an interchange mechanism, the actual BDE is higher than the measured value.

Table 3 Estimated bond dissociation energies of noble gas complexes

Ng–$M(CO)_5$	Bond dissociation energies (kcal mol^{-1})	Phase/ solvent	Ref.
Xe–$Cr(CO)_5$	9.0 ± 0.9	Gas	71
Xe–$Mo(CO)_5$	8.0 ± 1.0	Gas	71
Xe–$W(CO)_5$	8.2 ± 1.0	Gas	71
Kr–$W(CO)_5$	<6	Gas	71
Ar–$W(CO)_5$	<3	Gas	71
Xe–$W(CO)_5$	8.4 ± 0.2	Liq Xe	95
Xe–$W(CO)_5$	8.2 ± 0.2	sc Xe	96

4.4 Role of singlet and triplet structures for $Fe(CO)_4$ and related complexes

In the early days of carbonyl photochemistry, it was assumed that the initial stage of CO loss led to singlet states of metal carbonyl fragments. However, the matrix experiments on $Fe(CO)_4$, which demonstrated the importance of the triplet state, and subsequent experiments in the gas phase and solution, have shown that the photochemistry can be sensitive to the spin state. All the experiments show that there is no change of spin state prior to photodissociation but there may be a change in spin state after dissociation of CO. We now illustrate this with a few examples.

4.4.1 $Fe(CO)_4$. A striking application[31,97] of the combination of TRIR and supercritical solvents probed the singlet/triplet behaviour of $Fe(CO)_4$. On photolysing $Fe(CO)_5$ in scXe, the TRIR spectrum shows at 5 ps after the flash a clear example of the broadening of the C–O band due to the primary products being 'hot' (see above). Over time, the bands sharpen, and the bands of the ground state ^{3}**4** become clear (for nomenclature of $Fe(CO)_4$ and $Fe(CO)_3$, see Section 2.2). Fig. 2 shows the spectra at 25 and 200 ns, by which time the ^{3}**4** bands have disappeared and been replaced by the ^{1}**4-Xe** bands, exactly as expected on the basis of the matrix work (see above). What is interesting, though, is the observation of a band at 1926 cm^{-1}. In studies in cyclohexane, Bachler *et al.*[98] had seen the same band at about 0.4 μs after the flash, and which had disappeared by about 1.2 μs. Based on Poliakoff's matrix work[57] in a CH_4 matrix (a_1, 2040.1 (m); e, 1930.4 (s) cm^{-1}) this band was assigned to C_{3v} $Fe(CO)_3$, weakly coordinated to cyclohexane. This was a surprise because it implies that a single photon in solution can produce a loss of two COs. As far as we are aware, this was the first observation of this effect. In the scXe study,[31] the $Fe(CO)_3$ species is almost certainly interacting with Xe. In contrast to the behaviour in scXe, ^{3}**4** is readily seen at 500 ps in sc Ar and there is no evidence for conversion to any ^{1}**4-Ar**, again exactly as expected from the matrix work. The overall photochemistry is summarised in Scheme 10.

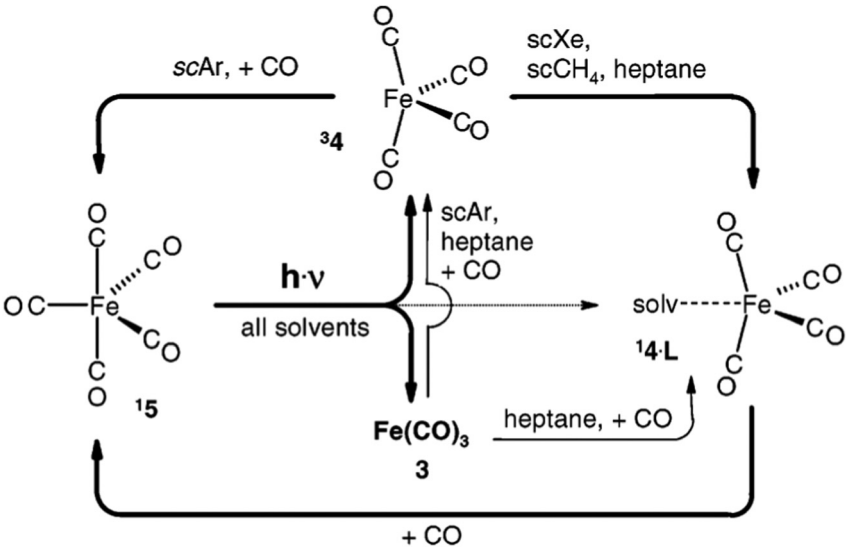

Scheme 10 Reactions of $Fe(CO)_5$, $Fe(CO)_4$ and $Fe(CO)_3$. The major reactions are indicated by thick arrows. Reproduced with permission from *J. Am. Chem. Soc.*, 2004, **126**, 10713–10720. Copyright 2004, American Chemical Society.[31]

4.4.2 CpCo(CO) and CpRh(CO). Photolysis of $CpCo(CO)_2$ yields CpCo(CO) with a triplet ground state, whereas $CpRh(CO)_2$ gives singlet CpRh(CO). Employing fs TRIR, Harris and colleagues[99] looked at reactions following UV photolysis of the parent complexes in triethylsilane. The basic reaction is shown on eqn (7).

$$\underset{M=Co,\,Rh}{CpM(CO)_2} \xrightarrow{h\nu,-CO} CpM(CO) \xrightarrow{+SiEt_3H} CpM(CO)(SiEt_3)H \quad (7)$$

However, surprisingly at first sight, the reaction of $SiEt_3H$ with the triplet is much faster than with the singlet. The proposed reason, based on studies in alkane solvents, is that the singlet rapidly coordinates to a C–H bond of an Et group, presenting a barrier to interaction with the Si–H bond. On the other hand, the triplet does not so coordinate, and *via* spin–orbit coupling is able to activate the Si–H bond.

4.4.3 $CpMn(CO)_2$. The photochemistry of $CpMn(CO)_3$ presents an interesting contrast. The first significant experiments were carried out employing TRIR on the fs time scale by Harris and colleagues.[100] These established that, on photolysis of $CpMn(CO)_3$ in *n*-heptane or triethylsilane, the triplet $^3[CpMn(CO)_2]$ is produced, and that this decays ($\tau \sim 100$ ps) to yield singlet $^1[CpMn(CO)_2(solvent)]$. This result encouraged McMahon and colleagues[58] to probe deeper into the matrix photochemistry of $CpMn(CO)_3$ (Section 2.2). In very recent work, George, Harvey and colleagues[33] confirmed Harris's observations, and, in addition, showed that in perfluoromethylcyclohexane (PFMCH) triplet $^3[CpMn(CO)_2]$ is first observed, and is converted to $^1[CpMn(CO)_2(PFMCH)]$. However, this reaction is much slower ($\sim$20 ns) than the corresponding heptane reaction. The photochemistry of $CpMn(CO)_3$ has attracted renewed interest with the demonstration that photolysis in biphasic water/hexane mixtures yields H_2 and H_2O_2 *via* $CpMn(CO)_2(H_2O)$.[101]

4.5 Combination of TRIR experiments with other techniques: NMR, RIXS and XFAS

4.5.1 NMR. The IR and UV spectroscopic methods, although providing evidence for metal–hydrocarbon and metal–noble gas interaction and reactivity, give no structural information concerning the interaction. Can the complexes be stabilised sufficiently to investigate by structure-sensitive methods? In the Gas Phase section we considered other techniques for investigating carbonyl photochemistry. Are there corresponding methods in solution? George *et al.*[102] had demonstrated *via* TRIR, that photolysis of $CpRe(CO)_3$ in *n*-heptane at room temperature produced $CpRe(CO)_2$(*n*-heptane) which was surprisingly long-lived (*ca.* 40 ms), reacting with CO *ca.* 400 times more slowly than $CpMn(CO)_2$(*n*-heptane). Geftakis and Ball reasoned that such species might be sufficiently long-lived at low temperature to be observed under continuous irradiation by NMR. In ground-breaking experiments they obtained the NMR spectrum[103] of $CpRe(CO)_2$(cyclopentane) at 180 K (see Section 6). The NMR experiments proved to be fully consistent with an η^2-C,H interaction with the metal. Later it proved possible to obtain the NMR spectra of $CpMn(CO)_2$(alkane) (alkane = propane, ethane, *n*-butane) even though these complexes required much lower temperature measurements and, even then, lasted only a few minutes.[104] The first NMR measurements of a methane complex were achieved by low temperature protonation of a rhodium complex.[105] Most recently, Ball has characterised $[CpOs(CO)_2(\eta^2\text{-}CH_4)]^+$ by NMR, following photolysis of $[CpOs(CO)_3]^+$ under CH_4 (Scheme 2).[4]

Ball, George and colleagues have also demonstrated the power of this technique with Xe complexes. Once again TRIR provided clues. Photolysis[102] of $CpRe(CO)_3$ in supercritical Xe at room temperature and liquid Xe at 170 K generated $CpRe(CO)_2Xe$, with a lifetime in the latter of about 3.5 min. Unfortunately $CpRe(CO)_3$ was insufficiently soluble in liquid Xe for NMR investigation. However, a combination of NMR and IR

positively identified[106] the coordinated xenon of (^{i}PrCp)Re(CO)(PF_3)Xe on photolysis of (^{i}PrCp)Re(CO)$_2$(PF_3) in liquid Xe *via* the couplings *J*(P–Xe), *J*(F–Xe) and the ^{129}Xe chemical shift.

4.5.2 Resonant inelastic X-ray scattering (RIXS). With the development of free-electron lasers it became possible to generate very short pulses (~150 fs) of X-rays in the hundreds of eV range. This leads to the possibility of studying short-lived transients by Resonant Inelastic X-ray Scattering (RIXS). Using this technique, it proved possible to follow some of the dynamics of the photoproducts following 100 fs irradiation at 266 nm of $Fe(CO)_5$ in ethanol.[107,108] The most important observations were: (a) the detection of the "hot" $^1A_1$ state of $Fe(CO)_4$; (b) the monitoring of the conversion of this state to either the $^3B_2$ ground state or its reaction with ethanol to give ^{1}Fe(CO)$_4$(ethanol); (c) the very fast appearance of the triplet because of interaction between the $^1A_1$ state and ethanol solvent molecules. These extremely difficult experiments add to previous work, but the broader application of RIXS to carbonyl photochemistry is in its infancy.

4.5.3 X-ray absorption fine structure spectroscopy (XAFS). Although UV/visible, TRIR and NMR provide valuable information of carbonyl photochemistry in solution, they cannot provide bond lengths. In principle, X-ray Absorption Fine Structure Spectroscopy (XAFS) can do that. Since many species of interest have limited lifetimes it is necessary to employ time-resolved XAFS, a difficult experiment.

In a remarkable paper, Cho *et al.* reported the time-resolved XAFS and XANES spectra of $Mn_2(CO)_{10}$, so obtaining the corresponding spectra of $Mn(CO)_5$ by difference (Fig. 11). The most significant change in the carbonyl geometry from $Mn_2(CO)_{10}$ to $Mn(CO)_5$ was the increase in C_{ax}–Mn–C_{eq} from 93.6 to 96.7°, respectively. (Unfortunately, no error bars are given.)[109] It will be recalled that the angle for $Mn(CO)_5$ determined from IR intensities[62] was 96 ± 3°, gratifyingly close!

Using a combination of XAFS with TRIR to provide spectroscopic data, it has recently been possible to determine the structures of the short-lived species W(CO)$_5$(heptane) and W(CO)$_5$Xe.[110] The most interesting parameter is the W–Xe bond length, 3.10 Å; a DFT calculation suggests a bond length of 3.15 Å. The same methods allowed determination of structural parameters for W(CO)$_5$(*n*-heptane) (Fig. 12).

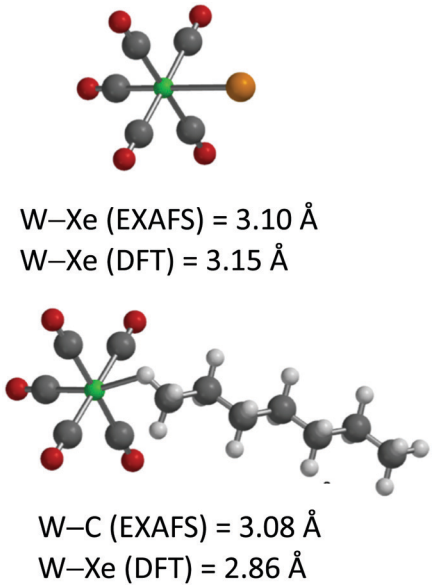

Fig. 12 Structures of W(CO)$_5$Xe and W(CO)$_5$(*n*-heptane) determined by EXAFS and DFT (LANL08 basis set for W and Xe, 6-311++G(d,p) for other atoms, M06 functional). Reproduced with permission from *J. Am. Chem. Soc.*, 2019, **141**, 11471–11480. Copyright 2019, American Chemical Society.[110]

Ultimately, one looks for single crystal X-ray diffraction to give accurate structures. This challenge was finally solved for alkane complexes by hydrogenation of a rhodium(diene) complex in a single crystal-to-single crystal transformation in which a single crystal of a diene complex is hydrogenated in the solid state to form the alkane complex while maintaining crystallinity.[111] These studies have provided metrical details of linear and cyclic alkanes acting as chelating ligands through two η^2-C,H linkages. Further information about alkane complexes is summarised in recent reviews.[111,112]

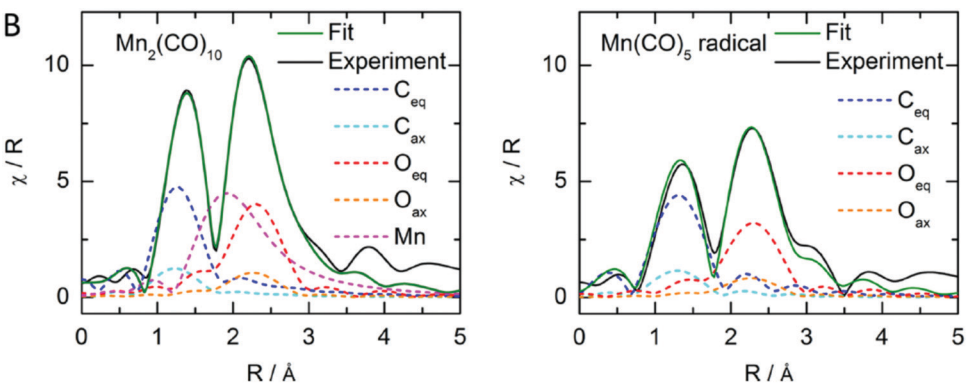

Fig. 11 XAFS spectra of $Mn_2(CO)_{10}$ and $Mn(CO)_5$ in propan-2-ol 400 ps after laser excitation at 400 nm. The diagrams show the Fourier transform experimental (black solid line) and fitted (green solid line) spectra and contributions from the scattering nuclei. Reproduced with permission from *Inorg. Chem.*, 2016, **55**, 5895–5903. Copyright 2016, American Chemical Society.[109]

Solution photochemistry: key points

(1) TRIR spectroscopy:
  (a) ns to ms for kinetics of reaction with substrates
  (b) fs to ps for:
    (i) initial photoproducts
    (ii) vibrational relaxation and geminate recombination
    (iii) reaction with solvent
    (iv) interconversion of product spin states
(2) Application of liquefied and supercritical noble gases as solvents.
(3) NMR, RIXS, XAFS provide direct evidence of coordination of Xe and alkanes.
(4) Dissociation of one CO group per photon absorbed typical; rare examples of two CO groups.
(5) Structures of unsaturated metal carbonyls in solution same as in matrices.
(6) Kinetics of Xe and alkane complexes, bond dissociation energies.
(7) Dinuclear metal carbonyls: CO loss and M–M cleavage as competing pathways with wavelength selective photochemistry.
(8) Coordinatively unsaturated metal carbonyls with Mn, Fe and Co may exist in triplet and singlet forms with different structures and reactivity.

5. Theory and gas-phase dynamics

How does theory relate to the structures and properties of the fragments generated by photolysis of metal carbonyls, and to the photochemical mechanisms? In this section we consider several questions: the shapes of carbonyl species; their energetics and C–O vibrational frequencies; the nature of excited states; the interaction with noble gases, and how photochemical excitation results in ultrafast and selective dissociation.

5.1 Structures and properties of the fragments generated by photolysis of metal carbonyls.

5.1.1 Shapes of fragments. If the question is the simple one of shapes, we need go no later than the mid 1970s. Burdett,[113] and Elian and Hoffmann[114] analysed the ground-state geometries of binary metal carbonyls by extended Hückel MO calculations. Burdett[115] also examined the geometries by looking at the competition between d-orbital stabilization energy and repulsion forces *via* angular overlap theory. Gratifyingly the results were essentially the same. The method considered the change in energy of the MOs as the bond angle between the CO groups changed, reminiscent of Walsh diagrams. As an example, consider $M(CO)_5$, with M = Fe, and M = Cr. Fig. 13 shows the change in energy levels going from a D_{3h} to a C_{4v} configuration *via* the C_{2v} configuration, that is along a Berry pseudo-rotation (for $Fe(CO)_5$ $[(e'')^4(e')^4,\ ^1A_1']$ to $[(b_2)^2(e)^4(a_1)^2,\ ^1A_1]$ *via* $[(a_2)^2(b_1)^2(b_2)^2(a_1)^2,\ ^1A_1]$.[116] The most stable structure for d^8 $Fe(CO)_5$ is D_{3h}, but the C_{4v} structure is only a little higher in energy. The latest measurement of the barrier,[117] estimated from the changes in C–O FTIR spectral changes with temperature, is 2.5 ± 0.4 kcal mol^{-1}. DFT calculations[117,118] suggest a barrier height of about 2.2 kcal mol^{-1}. On the other hand, d^6 $Cr(CO)_5$ is predicted to have a C_{4v} structure $[(b_2)^2(e)^4,\ ^1A_1]$ as is indeed the case.[39] It is worth noting that both $Mn(CO)_5$ (see above) and isoelectronic $[Cr(CO)_5]^-$,[119] have C_{4v} structures $[(b_2)^2(e)^4(a_1)^1,\ ^2A_1]$ in line with the Burdett/Hoffmann model. Moreover, a D_{3h} structure

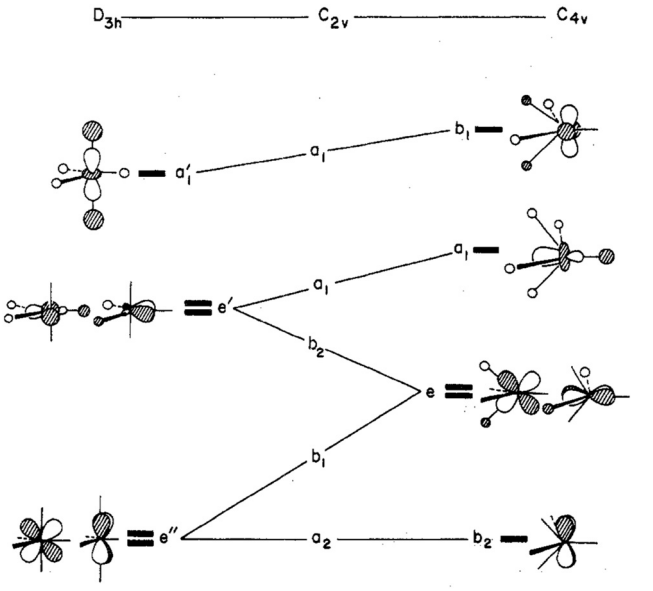

Fig. 13 Wave function and energy changes along a Berry pseudorotation for $M(CO)_5$. Reproduced with permission from *Inorg. Chem.*, 1975, **14**, 365–374. Copyright 1975, American Chemical Society.[116]

$[(e'')^4(e')^3]$ would be Jahn–Teller unstable. These MO calculations also explain the C_{2v} structures of $Mo(CO)_4$ and $Fe(CO)_4$ (both singlet and triplet), and the C_{3v} structures of $Fe(CO)_3$ and $Mo(CO)_3$. Notice the importance here of considering electronic states, not just orbital populations. Thus theory demonstrates that the structures of metal carbonyl fragments $M(CO)_n$ are determined by the number of CO groups n, and the d-electron count.

The invention of DFT methods has brought much more quantitative calculations within reach and has stimulated a great deal of theory on metal carbonyls and their photochemistry.[120] Of particular relevance are calculations on the primary photoproducts of $Cr(CO)_6$ and $Fe(CO)_5$, *i.e.* $Cr(CO)_5$ and $Fe(CO)_4$.[121] Full *ab initio* (*e.g.* CCSD(T)) calculations on large molecules are very expensive, but they are now within reach for some problems.[122,123] As mentioned earlier, the problem with DFT calculations is that the results – especially bond angles and C–O stretching frequency – can be sensitive to the functional.

5.1.2 Calculation of vibrational frequencies. We first consider vibrational frequencies. There is a particular problem with predicting frequency, in that most calculations supply harmonic frequencies, whereas most experimental studies involve anharmonic frequencies. Moreover, a 'scaling' factor is usually applied to bring the calculated CO-stretching frequencies into line. There is an amusing comment in the Supporting Information of a paper by Ihee and colleagues.[120] "Since the theoretical methods generally overestimate the C–O stretching frequency, direct comparison between the values from experiment and computation is not relevant. Therefore, certain scaling factors are needed to correct the calculated vibrational frequencies, but they are not available for all DFT functionals at the moment." A striking example of this problem is demonstrated in the earlier paper by the same authors.[124] It is possible to do anharmonic calculations, but they are rarely

reported probably because they are very time-consuming.[125,126] DFT calculations commonly have discrepancies between observed and calculated frequencies of tens of cm^{-1} even after scaling; the discrepancies may vary greatly even between different modes of the same molecule.§ Nevertheless, many authors find that, with care, they can be used effectively to guide assignments.[10] In contrast, the EFFF typically models the frequencies with RMS differences of *ca.* 2 cm^{-1}.

5.1.3 Energetics of ground and excited states. Why do coordinatively unsaturated 16e- and 14e-metal carbonyls exhibit lower-lying electronic absorption bands than their closed-shell 18e-counterparts? A comparison of d^6 $Cr(CO)_5$ provides a simple qualitative explanation. The 3d (t_{2g}) orbitals of $Cr(CO)_6$ are π-bonding, but split into an e and b_2 set for $Cr(CO)_5$ with correspondingly reduced π-bonding. The empty 3d (e_g) set are σ-antibonding and split into an a_1 (d_{z^2}) and b_1 ($d_{x^2-y^2}$) orbital, with the a_1 orbital lying at lower energy than the e_g orbital of $Cr(CO)_6$ (see Fig. 13 right). Moreover, the a_1 (d_{z^2}) orbital can mix with the empty $4p_z$ orbital, reducing its energy even further.[114] Consequently, there is a transition from the occupied e orbital to the empty a_1 orbital at low energy that appears at 624 nm (16 000 cm^{-1}) in a neon matrix – compare the lowest energy absorption band of $Cr(CO)_6$ at 340 nm (29 000 cm^{-1}). Translated into electronic states, this is the transition from the ground $^1A_1$ state to the excited ^1E state (see Fig. 7). The reduced symmetry and reduced number of CO groups means that low-lying electronic transitions are ubiquitous for coordinatively unsaturated metal carbonyls.

This analysis shows that – ignoring the triplet states, to which we will return – the lowest energy transition of $Cr(CO)_5$ is from $^1A_1$ to the ^1E state. However, this C_{4v} excited state is unstable with respect to D_{3h} [$(e'')^4(e')^2$, *i.e.* $^1E'$)]. In turn, this excited state is unstable in turn with respect to the ground state C_{4v} structure [$(b_2)^2(e)^4$; $^1A_1$] (Fig. 7 and 13). Thus with this simple model we can explain why irradiation into the lowest absorption band of $Cr(CO)_5$ in a matrix leads to a Berry pseudorotation (see Section 2).

A paper[121] which is useful for providing earlier references, employs three popular DFT functionals (B3LYP, BP86, M06-L) to examine, among other systems, $Cr(CO)_5$ and $Fe(CO)_4$. We can summarise the energy level situation, in kcal mol^{-1}, for $Cr(CO)_5$ with approximate values based on a variety of calculations (Table 4).

Elian and Hoffmann pointed out that the mixing of the empty d_{z^2} and p_z orbitals of $Cr(CO)_5$ generates a low-lying orbital, perfectly adapted for turning it into a powerful Lewis acid.[114] Does this account for the formation of alkane complexes and noble gas complexes, probably yes for the former but perhaps not for the latter? Both *ab initio* and DFT calculations were carried by Ehlers *et al.* on $M(CO)_5Ng$. This important work[127] argued that the interaction involved van der Waals forces rather than genuine chemical bonds between the metal and the noble gas. A critical part of the original experimental evidence depended on the shifts in the energy of the excited ^1E state with Ng. A further impressive part of this paper is that time-dependent DFT calculations of the $^1A_1 \rightarrow {}^1E$ ($e^4a_1{}^0 \rightarrow e^3a_1{}^1$) transitions in $Ng–Cr(CO)_5$ match closely those observed in the matrix (Table 5).[40] The match with the Mo and W complexes was much less impressive.

Table 4 Electronic states and energies of $Cr(CO)_5$

Symmetry	d orbital occupancy	Electronic state	Energy (kcal mol^{-1})
C_{4v}	$[(b_2)^2(e)^3(a_1)^1]$	^1E	45
D_{3h}	$[(e'')^4(e')^2]$	$^1E'$	25
C_{4v}	$[(b_2)^2(e)^3(a_1)^1]$	^3E	17
D_{3h}	$[(e'')^4(e')^2]$	$^3A_1'$	12
C_{4v}	$[(b_2)^2(e)^4]$	$^1A_1$	0

Table 5 Experimental and calculated wavelengths of visible absorption of $Ng–Cr(CO)_5$ (Ng = noble gas)

	Wavelength (nm) of $^1A_1 \rightarrow {}^1E$ transition			
	$Ne–Cr(CO)_5$	$Ar–Cr(CO)_5$	$Kr–Cr(CO)_5$	$Xe–Cr(CO)_5$
Experiment[40]	624	533	518	492
Theory[127]	653[a]	523	516	504

[a] For naked $Cr(CO)_5$.

5.2 Mechanisms of photodissociation of $M(CO)_6$ (M = Cr, Mo, W)

But how does the photochemistry of the parent proceed? There have been an enormous number of UV/vis absorption studies on transition metal carbonyls; for our present purposes, the important point is that it has now been demonstrated conclusively by time-dependent DFT methods[128,129] that the ligand field (LF) excited states of $M(CO)_6$ molecules are at higher energy than metal-to-ligand charge transfer states (MLCT), contrary to what was originally thought. Moreover, there is also strong support from experiment.[130] Thus, UV irradiation will populate MLCT states. However, although LF states are expected to lead to dissociation of CO groups, this is not the case for MLCT states. Given the high quantum yield for CO dissociation, this is at first rather puzzling. The calculations showed that that the relative energies of states change as the molecules distort and the MLCT state formed initially crosses into a LF state which is dissociative. Notice that there is no change in spin state. Elegant gas-phase experiments by Fuss and colleagues offer a detailed explanation of this result.[131]

With the hexacarbonyls $M(CO)_6$ (M = Cr, Mo, W), pulsed UV lasers (270–345 nm; approx. lifetime 30 fs) excite the molecules and the resulting dissociation is probed with non-resonant ionization (810 nm; 20 fs). The cations $M(CO)_x^+$ are analysed in a time-of-flight mass spectrometer. The repulsive LF state ejects a CO, leading to C_{4v} $M(CO)_5$ in an excited ^1E state (Fig. 14). What then follows, as the authors point out, matches the previous conclusions, in particular the matrix polarisation experiments.[41]

In other words, this is dissociative photochemistry with no time to form equilibrated excited states. This experiment

§ Inaccuracies in vibrational frequencies also affect calculations of free energies *via* the third law of thermodynamics which require knowledge of the zero-point energy.

confirms the matrix experiments which implied that the C_{4v} ^{1}E excited state is unstable with respect to the D_{3h} ^{1}E′ state distorted form of $M(CO)_5$ and this, in turn, relaxes to the $^1A_1$ C_{4v} ground state structure. Photodissociation dynamics calculations[132] have fleshed out the details of formation of $Cr(CO)_5$ in its ^{1}E excited electronic state within *ca.* 80 fs of excitation of $Cr(CO)_6$ and how it crosses through the conical intersection into the ground state creating oscillations between trigonal bipyramidal and square pyramidal geometries corresponding to the Berry pseudorotation, very much as postulated in qualitative form 24 years earlier.

There is an alternative pathway in the gas phase. There may be sufficient energy in the $M(CO)_5$ fragment to lead to further loss of CO groups, the number depending on the original laser wavelength. The interesting fact is that the generation of $M(CO)_n$ fragments involves only one photochemical act, the loss of a single CO from the parent. The loss of multiple CO groups contrasts with what usually happens in solution, where rapid collisions disperse the excess energy before the molecule can further dissociate.

As we described earlier, $Cr(CO)_5L$ complexes (L = Xe, CH_4, phosphine, *etc.*) undergo wavelength-selective photochemistry. On irradiation at long wavelength, only the ligand L is ejected, while at shorter wavelength CO ejection is dominant. Why do they show this behaviour which is quite unlike that of most organic molecules? Baerends and colleagues[133] by time-dependent DFT have shown the lowest excited state of $Cr(CO)_5(PH_3)$ to be MLCT in character while the LF state formed by population of the d_{z^2} orbital lies above it. However, as soon as the Cr–P bond lengthens, the states undergo an avoided crossing which occurs within the Cr–PH_3 and beyond the Cr–CO equilibrium distances. The result is PH_3 dissociation but a barrier remains for CO dissociation. This dissociation generates the first excited state of $Cr(CO)_5$, so the same dynamics will ensue as described for $Cr(CO)_6$ photodissociation, albeit with less excess energy. The occurrence of wavelength dependent photochemistry for $Cr(CO)_5L$ and other examples below depends on dissociation on an ultrafast timescale before the molecule can equilibrate with its surroundings.

5.3 Electronic states of $Fe(CO)_4$, role of singlets and triplets, photochemical mechanisms for $Fe(CO)_5$

We now turn to $Fe(CO)_4$, for which the calculated energy levels[119] are shown in Scheme 11.

The first interesting point to note is that there is an isomerisation process in $Fe(CO)_4$ analogous to the Berry pseudorotation in $Fe(CO)_5$. This process can be induced by IR laser irradiation in one of the C–O IR bands of ^{13}CO-enriched $Fe(CO)_4$ trapped in a low-temperature matrix.[134,135] Moreover it was shown that the

C_{2v}	$^1B_2$	----------	30
C_{2v}	$^1A_1$	----------	18
C_{2v}	$^3B_2$	----------	0

Scheme 11 Electronic states and calculated energies (kcal mol^{-1}) of $Fe(CO)_4$.

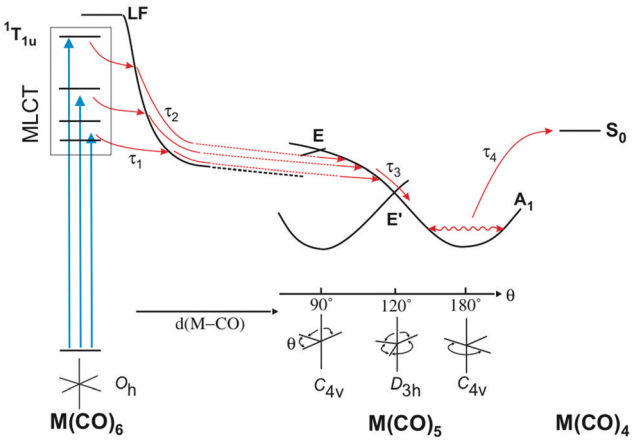

Fig. 14 Three different laser wavelengths (270, 318 and 345 nm) excite $M(CO)_6$ into MLCT states. There is then extremely rapid crossing (12.5 fs) to the repulsive LF state. See the text for the next steps. *Chem. Phys.*, 2008, S. A. Trushin, K. Kosma, W. Fuss and W. E. Schmid, "Wavelength-independent ultrafast dynamics and coherent oscillation of a metal–carbon stretch vibration in photodissociation of $Cr(CO)_6$ in the region of 270–345 nm", **347**, 309–323, Copyright 2008, with permission from Elsevier.[131]

mechanism of this process involves the very rare non-Berry pseudorotation (Fig. 15). Since an IR frequency of 2000 cm^{-1} corresponds to an energy of 5.7 kcal mol^{-1}, this value represents an upper limit for this process. On the other hand, in the presence of L = CH_4 or Xe, the interaction energy is sufficient to cause reaction to the more stable ^{1}[$Fe(CO)_4$L], which is lower in energy than the $^3B_2$ ground state of the 'bare' $Fe(CO)_4$ (see Scheme 6). Whether the triplet or singlet states are experimentally observed, depends on timescales.

Both the ground triplet and the excited singlet states of $Fe(CO)_4$ have C_{2v} structures, but with different bond angles. The paper by Sun *et al.* reports calculated bond angles of $Fe(CO)_4$ obtained with several functionals (Table 6). For the $^1A_1$ state, there is an excellent match between the calculated[121] and experimental[52,56] values. For the $^3B_1$ state, there is some discrepancy which will not be resolved until there is new experimental evidence.

We turn to the photochemistry of the parent, $Fe(CO)_5$. It is more complex than $Cr(CO)_6$ for two reasons: the initially excited states are mixed in character and the ground states of $Fe(CO)_4$ and $Fe(CO)_3$ are triplets. Nonetheless the overall pattern is very similar. Fig. 16 shows part of the proposed pathway.[136] After loss of a CO, $Fe(CO)_4$ is generated in an excited C_{2v} **singlet** ($^1B_2$), which *via* the tetrahedral $^1T_2$ state, relaxes to the **singlet** C_{2v} $^1A_1$ state, which is still electronically excited. This is the state observed by Zewail by electron diffraction. Weitz and

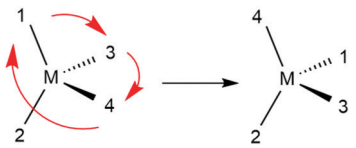

Fig. 15 A permutation of three ligands consistent with the non-Berry pseudorotation. Adapted with permission from *J. Am. Chem. Soc.*, 1984, **106**, 50–54. Copyright 1984, American Chemical Society.[135]

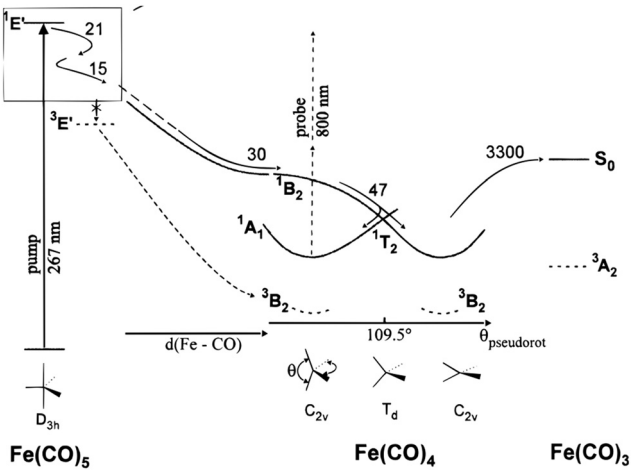

Fig. 16 The photodissociation of $Fe(CO)_5$; times in fs. Reproduced with permission from *J. Phys. Chem A*, 2000, **104**, 1997–2006. Copyright 2000, American Chemical Society.[136]

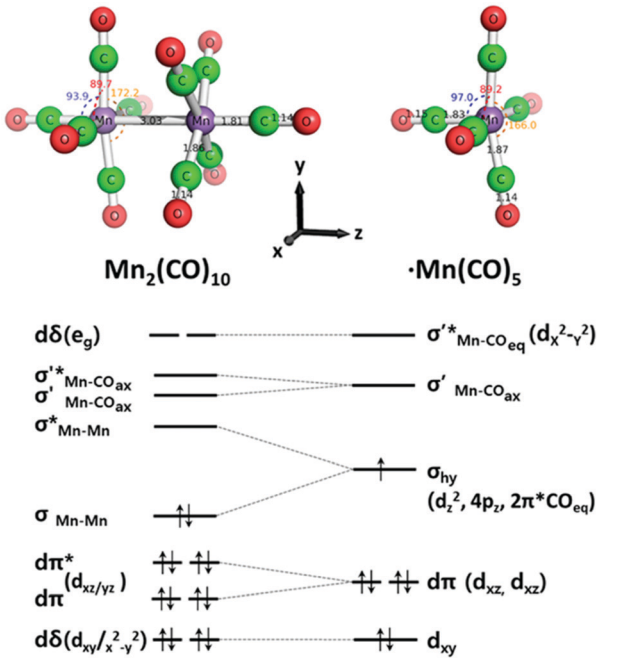

Fig. 17 DFT optimised structures for $Mn_2(CO)_{10}$ in D_{4d} and $Mn(CO)_5$ radical in C_{4v} symmetries with selected calculated bond angles and lengths. At the bottom are shown simplified MO diagrams with dominant metal contributions. Reproduced with permission from *Inorg. Chem.*, 2016, **55**, 5895–5903. Copyright 2016, American Chemical Society.[109]

colleagues, following their early TRIR experiments in which they only observed the triplet ground state ($^3B_2$),[69] were also able to detect the excited singlet state.[137] The relaxation from **singlet** to ground state **triplet** ($^3B_2$) takes >500 ps, which is why it was not observed in Zewail's studies.[55]

The magnitude of the triplet-singlet gap is not known experimentally and is extremely hard to determine computationally. Reactions involving a change of spin-state such as $^1[Fe(CO)_4] \rightarrow {}^3[Fe(CO)_4]$ or $^3[Fe(CO)_4] + L \rightarrow {}^1[Fe(CO)_4L]$ (L = CO, Xe, H_2) are enabled by spin–orbit coupling. One approach to obtaining the barrier is to calculate the potential energy surfaces of the reactant and product along the appropriate coordinates and hence determine the minimum energy crossing point between them. This method has had considerable success, but there are subtleties in putting it into practice.[97,138] A multidimensional method reports better agreement with experiment for the reaction with H_2 but does not calculate the rate constant.[139]

Baerends *et al.*[133] have also addressed the preference for PH_3 dissociation for ax-$Fe(CO)_4(PH_3)$ and shown by quantum dynamics that there is a strong preference for dissociation of PH_3 over CO on population of the lowest excited state, but the details are different from those described for $Cr(CO)_5PH_3$. The theory of H_2 dissociation from $Fe(CO)_4(H)_2$ has been addressed by Daniel[140] by CASSCF methods. There are two singlet excited states accessed by UV irradiation $^1B_1$ (d_{yz} to σ_g^*) and $^1A_1$ ($3d_{x^2-y^2}$ to σ_g^*) where σ_g^* is Fe···H_2 antibonding but H···H bonding. Elimination of H_2 occurs within tens of femtoseconds in preference to dissociation of CO without intersystem crossing. The paper also addresses the reverse reaction on visible excitation of $Fe(CO)_4$.

5.4 Photochemical mechanisms for $Mn_2(CO)_{10}$

The theory of the photochemistry of $Mn_2(CO)_{10}$ needs to explain why there are two competing dissociation processes with relative quantum yields that depend on irradiation wavelength and how the bridging ligand of $Mn_2(CO)_9$ is formed. Detailed DFT calculation by Baerends and colleagues[141,142] have established an appropriate energy-level diagram and explained the photochemistry. A simplified diagram, based on Baerends' work, is described in a later paper (Fig. 17).[109] Low energy (337–355 nm) UV irradiation promotes the $\sigma \rightarrow \sigma^*$ transition ($^1A_1 \rightarrow {}^1B_2$) which, *via* intersystem crossing, reaches the Mn–Mn dissociative $^3B_2$ state; this produces two $Mn(CO)_5$ radicals in their $^2A_1$ ground states. To eject a CO group, higher energy UV is necessary, and the full picture is complex.[141] The calculations suggest that the stable form of $Mn_2(CO)_9$ has the semibridging structure, $(OC)_4Mn(\mu\text{-}CO)Mn(CO)_4$, as determined by the matrix isolation and TRIR experiments described earlier. However, as stated above, this cannot be the primary step in the photolysis. The authors suggest that the first step involves loss of an axial CO group, followed by the extremely fast rearrangement to the bridging structure. Cho *et al.* describe

Table 6 Bond angles of $Fe(CO)_4$

Method	Ground state (C_{2v}; $^3B_1$)	Excited state (C_{2v}; $^1A_1$)	Ref.
DFT calcd, various functionals	146 to 151 and 97 to 98	157 to 168 and 132 to 128	121
Exptl IR C–O intensities	145 and 120	173 and 125	52
Exptl gas electron diffraction		169 and 125	56

the time-resolved XANES and XAFS study of both $Mn_2(CO)_{10}$ and $Mn(CO)_5$, irradiating at 400 nm in the long-wavelength edge of the band (Section 4.5.3).[109] The XANES spectra are analysed by comparison with TD-DFT calculations to show details of the electronic structure of $Mn(CO)_5$.

5.5 Alternative types of metal carbonyl photochemistry

The principles of dissociative photochemistry outlined above can be extended to numerous substituted metal carbonyls but not to all. While cyclopentadienyl metal carbonyls follow the same pattern, there are some arene-substituted metal carbonyls and numerous diimine-substituted metal carbonyls that do not (diimine includes bipyridine, phenanthroline, *etc.*). The arene complexes (η^6-arene)$M(CO)_3$ (M = Cr, Mo) exhibit both CO dissociation and arene dissociation in different ratios according to solvent (see Fig. 3).[32,143,144] Moreover, CO dissociation may be ''delayed'' for tens of picoseconds.[2]

A further group of complexes exhibits dissociative photochemistry, but not of the CO ligands. Thus, irradiation of $Ru(CO)(PPh_3)_3(H)_2$ results in reductive elimination of H_2 and competing dissociation of PPh_3 but there is no loss of CO.[145] Similar behaviour has been observed for other metal monocarbonyl dihydride complexes.[2]

Diimine-substituted metal carbonyls usually exhibit quite different photochemical behaviour with long-lived (nanosecond) equilibrated excited states of charge-transfer character that are emissive and redox active. The application of $[Re(CO)_3(2,2'\text{-bipy})L]^{+/0}$ complexes has proved exceptionally important.[2] An early experiment[146] showed that it was possible to probe, by TRIR, the long-lived excited state of $[ClRe(CO)_3(4,4'\text{-bpy})_2]$; electron transfer from Re to the organic ligand results in an effective oxidation of the Re, and consequently an upward shift in the C–O IR bands. Since then there has been a plethora of experiments exploiting the application of a variety of time-resolved spectroscopies to excited states and corresponding investigation by theory.[2,32,147] Recent examples of IR, Raman and X-ray methods also involve DFT calculations.[148–150]

Theory and dynamics: key points

(1) Theoretical structures of metal carbonyl fragments $M(CO)_n$ agree with experiment and depend on n and the d-electron count.
(2) CO stretching frequencies difficult to reproduce accurately by computation.
(3) Lower symmetry and reduced n results in low-lying excited states for 16e and 14e-$M(CO)_n$ compared with 18e species.
(4) Photodissociation of CO depends on excitation into MLCT excited state followed by ultrafast (femtosecond) crossing into dissociative LF state.
(5) Dissociation proceeds through excited electronic states of the photoproduct.
(6) The wavelength dependence of the photochemistry of $Cr(CO)_5L$ and $Mn_2(CO)_{10}$ depends on ultrafast branching leading to dissociation down competing channels.
(7) The spin state may change after dissociation as in $Fe(CO)_4$ but not before.
(8) Femtosecond dissociation is not universal for metal carbonyls. Three classes of exception:
(a) (η^6-arene)$M(CO)_3$ (M = Cr, Mo) lose CO more slowly
(b) metal monocarbonyl dihydrides lose H_2 on irradiation
(c) complexes with low-lying excited states involving charge transfer to non-carbonyl ligands such as diimines exhibit equilibrated excited states

6. Applications to synthesis of complexes with labile ligands

6.1 Importance of labile ligands.

We have already seen that reactive intermediates such as $Cr(CO)_5$ coordinate solvent molecules on an ultrafast timescale and that their lifetime with respect to re-coordination of CO is strongly dependent on the coordinating ligand. Examples encountered so far include alkane complexes, noble-gas (Ng) complexes and the short-lived perfluoroalkane complexes. We have also seen the rapid conversion of $Cr(CO)_5(\eta^2$-benzene) to $Cr(CO)_5(THF)$. Thus, photodissociation of metal carbonyls is an excellent method for investigating the ability of these unusual ligands to form labile complexes. Are such complexes important? The alkane complexes have acted as paradigms for the development of σ-bond complexes,[151] while the $Cr(CO)_5Xe$ and $Fe(CO)_4Xe$ were the first examples of the metal–Ng bond. These complexes also have a role in synthesis since they prolong the lifetime of the reaction intermediates giving them sufficient time to react with solutes that may be present in lower concentrations. The classic synthetic method of forming $Cr(CO)_5(THF)$ photochemically and then replacing THF with another ligand in a thermal reaction is an example of such a strategy but is limited to the formation of less labile complexes than $Cr(CO)_5(THF)$. In this section, we examine the photochemical method for the formation of N_2 and H_2 complexes as well as labile metal alkyl hydride complexes, concentrating on information that has not been obtained by conventional synthetic methods. Photochemistry in organic solvents is limited by the low solubility¶ of N_2 and H_2. This limitation is removed in liquefied noble gases under pressure where N_2 and H_2 have much higher solubility than in most conventional solvents under similar conditions.

6.2 Examples of dinitrogen complexes

N_2 is isoelectronic with CO, but the transition metal complexes with N_2 as ligand are much less stable than metal carbonyls. The first metal carbonyl, $Ni(CO)_4$, was synthesised in 1890 but it was a further 75 years before the first stable N_2 complex, $[Ru(N_2)(NH_3)_5]^{2+}$, was made.[152] The first successful attempt to form a dinitrogen complex by matrix photochemistry was Rest's generation of $Ni(CO)_3(N_2)$ by photolysis of $Ni(CO)_4$ in a $^{14}N_2$ matrix (1/5000) at 20 K. As well as IR bands readily assigned to the $Ni(CO)_3$ group, a band at 2266 cm^{-1}, which shifted to 2193 cm^{-1} when the experiment was repeated in a $^{15}N_2$ matrix, was clearly identified with the N–N stretching vibration.[153] It proved possible to generate this unstable species by photolysis of $Ni(CO)_4$ in N_2-doped liquid Kr, and identify it by comparison with the matrix data. In the presence of added CO, the reverse reaction readily occurred and by monitoring this reaction over the temperature range 112–127 K, a Ni–N_2 bond dissociation energy of at least ~10 kcal mol^{-1} was estimated.[154]

In a similar manner, by a combination of matrix isolation and liquefied noble gas solvents, it proved possible to generate

¶ Solubilities of N_2 and H_2 in heptane 9.5×10^{-3} and 4.5×10^{-3} M at 1 atm, respectively.

all the species $Cr(CO)_{6-x}(N_2)_x$ (x = 1 to 5).[155] As photolysis proceeds in N_2-doped liquid Xe at 194 K, the degree of substitution increases. The assignment of the individual species was enormously helped by employing the EFFF approximation technique introduced by Timney.[25] Even now, we know of no other solution observations of a complex with five N_2 ligands.

The formation of $Cr(CO)_5(N_2)$ has been examined by TRIR of $Cr(CO)_6$ in N_2-saturated cyclohexane at room temperature. As expected, the first identified transient is $Cr(CO)_5$(cyclohexane) which converts to $Cr(CO)_5(N_2)$ with a first order rate constant of $\sim$18 000 s^{-1}. At room temperature, the $Cr(CO)_5(N_2)$ has a lifetime of about 1 s.[156] By employing photoacoustic calorimetry, Walsh *et al.* estimated the Cr–N_2 bond energy of $Cr(CO)_5(N_2)$ as $\sim$19 kcal mol^{-1}.[157]

Many other such photochemical reactions have been carried out to generate species of varying degrees of stability.[158] In the most recent example, the photolysis of Mn(C^N)$(CO)_4$ (C^N = bis-(4-methoxyphenyl)methanimine), was examined by ultrafast TRIR in both pure heptane, and in heptane under an atmosphere of N_2. In pure heptane, at $<$2 ps, the spectra displayed the usual 'hot' features which relaxed to show at $\sim$10 ps C–O IR features readily assigned to Mn(C^N)$(CO)_3$(heptane). Under N_2, the species Mn(C^N)$(CO)_3(N_2)$ was formed from the solvent complex in $\sim$20 ns.[159]

6.3 Examples of dihydrogen complexes.

Kubas' discovery in 1984 that transition-metal compounds could not only bind hydrogen as hydride but also as dihydrogen ligands, marked a seminal moment in coordination chemistry.[160,161] The photochemistry of metal carbonyls that include hydride ligands has been reviewed.[162] Kubas' original experiment reported the formation of $W(CO)_3(PR_3)_2(\eta^2\text{-}H_2)$ from thermal reaction of H_2 with $W(CO)_3(PR_3)_2$ (R = cyclohexyl, ^{i}Pr). We describe some experiments which demonstrate the photochemical generation of dihydrogen complexes from metal carbonyls.

Although photolysis of $Cr(CO)_6$ in H_2-doped Ar matrices provided strong evidence for the formation of an H_2 species, there was scant information from any vibrations involving an attached H_2 group.[163] However, photolysis of $Cr(CO)_6$ in H_2- and D_2-doped liquid Xe at 200 K, produced convincing evidence from the H–H and D–D stretching vibrations at 3030 and 2242 cm^{-1} respectively, of the formation of $Cr(CO)_5(H_2)$.[164] Moreover the position of the C–O bands was consistent with this species rather than the dihydride $Cr(CO)_5(H)_2$. The H–H and D–D stretching modes are broadened because of internal rotation of the dihydrogen ligand. Under the conditions of this experiment, the product is thermally quite stable although isotopic exchange of coordinated H_2 occurs under D_2. In contrast, TRIR of $Cr(CO)_6$ in H_2-saturated cyclohexane at room temperature, shows that $Cr(CO)_5(H_2)$ decays with a rate constant of 2.5 s^{-1}.[165] Further experiments showed the generation of the corresponding Mo and W species as well as $Cr(CO)_4(H_2)_2$.[164] Subsequently, $M(CO)_5(H_2)$ (M = Cr, W) complexes were characterised by NMR spectroscopy following photolysis of $M(CO)_6$ at 195 K in several solvents under 1.5 atm H_2.[166] The role of dihydrogen complexes is illustrated by the unusual product distribution in the photocatalytic hydrogenation of norbornadiene (NBD) by $Cr(CO)_6$ which proceeds initially *via* $Cr(CO)_4(\eta^4\text{-NBD})$. The latter is converted to two isomers of $Cr(CO)_3(\eta^4\text{-NBD})$(solvent) followed by the corresponding dihydrogen complexes $Cr(CO)_3(\eta^4\text{-NBD})(H_2)$, one of which generates norbornene and the other nortricyclene.[167]

The reactions of $CpM(CO)_4$ with H_2 in liquefied Xe are of particular interest because of the changes in product distribution. For M = V the only product is $CpV(CO)_3(H_2)$, for M = Ta only the dihydride $CpM(CO)_3(H)_2$ is formed, while for M = Nb both dihydrogen and dihydride complexes are formed. The highest wavenumber a′ C–O stretch is shifted down *ca.* 30 cm^{-1} with respect to $CpM(CO)_4$ for dihydrogen complexes whereas that of the dihydride complexes is shifted up by *ca.* 15 cm^{-1} in accord with the increased oxidation state The H–H stretching mode is observed as a broad band at *ca.* 2600 cm^{-1}. The dihydrogen and dihydride complexes of niobium lie at rapid equilibrium, with a standard enthalpy of 3.5 $\pm$ 0.5 kJ mol^{-1} in favour of $CpNb(CO)_3(H_2)$.[168]

6.4 The link between C–H oxidative addition and alkane coordination.

There was great excitement in 1982 when the activation of saturated hydrocarbons to produce alkyl complexes was demonstrated.[169,170] The work by Hoyano and Graham (eqn (8)) is particularly relevant to this Review since it involved the photolysis of a metal carbonyl in neopentane to form the product of oxidative addition:[170]

$$Cp^*Ir(CO)_2 \xrightarrow[-CO]{h\nu,\, C(CH_3)_4} Cp^*Ir(CO)\{CH_2C(CH_3)_3\}H \qquad (8)$$

$$Cp^* = \eta^5\text{-}C_5Me_5$$

Graham and colleagues even managed to activate methane, by photolysis of $Cp^*Ir(CO)_2$ in CH_4-doped perfluorohexane to give $Cp^*Ir(CO)(H)(CH_3)$.[171] This was a clever experiment. Graham did not have the facilities for working in liquid or supercritical CH_4, but from the matrix and liquid perfluoro experiments, it was known that the perfluoro solvent binds less strongly to a carbonyl fragment than a hydrocarbon, so the CH_4 displaces the perfluoro solvent as ligand. These oxidative addition reactions are characteristic of the 4d and 5d metals of group 8 and 9 that form d^8 reaction intermediates, with a few examples from group 7. The obvious route involves the photoactivated loss of CO to form the unsaturated $Cp^*Ir(CO)$ intermediate which then reacts with the hydrocarbon. By analogy with the oxidative addition of H_2, it might be surmised that the mechanism involves a species in which a C–H bond forms an $Ir(CH_4)$ complex. As described in previous sections, there is plenty of evidence that metal carbonyl fragments interact quite strongly with saturated hydrocarbons such as cyclohexane.

Meanwhile, the question is: can an alkane complex be identified, and can its conversion to the alkyl hydride be observed and monitored? By analogy with earlier work, the matrix technique might be one method of following this. In matrix photolysis experiments on $Cp^*Ir(CO)_2$ in CH_4 at 12 K, Rest *et al.* easily observed the activated species, *i.e.* $Cp^*Ir(CO)(H)(CH_3)$. Moreover, oxidative addition of methane was also observed with $CpIr(CO)_2$, $Cp^*Rh(CO)_2$ and $CpRh(CO)_2$.[172] Notably the reaction

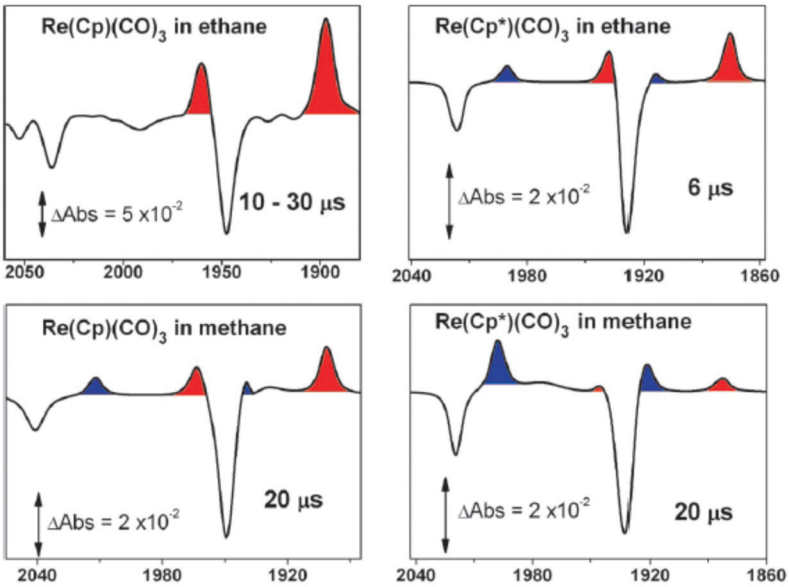

Fig. 18 IR difference spectra recorded at the time delays shown after photolysis of indicated species in ethane (114 bar) or methane (276 bar) in the presence of CO at room temperature. Red and blue shaded areas indicate ν(CO) bands of $CpRe(CO)_2$(alkane) and $CpRe(CO)_2$(alkyl)(H), respectively. *Proc. Natl. Acad. Sci. U. S. A.*, 2007, **104**, 6933–6938, Copyright 2007 National Academy of Sciences.[175]

proceeded in much higher yield starting from $CpIr(CO)(H)_2$, but evidence for $CpIr(CO)(CH_4)$ was not decisive.[173] An ultrafast TRIR study on $CpIr(CO)_2$ in cyclohexane showed that the risetime of the CpIr(CO)(cyclohexyl)(H) was as short as 2 ps and no cyclohexane complex was observed.[174]

In contrast, George *et al.*'s TRIR study on $Cp^*Re(CO)_3$ and $CpRe(CO)_3$ in supercritical methane and ethane demonstrated formation of a methane complex prior to the corresponding methyl hydride complex.[175] Irradiation of $Cp^*Re(CO)_3$ in sc CH_4 shows $Cp^*Re(CO)_2(CH_4)$ after a few picoseconds together with vibrationally excited $Cp^*Re(CO)_3$. Monitoring over the subsequent nanoseconds shows the partial conversion (Fig. 18) of $Cp^*Re(CO)_2(CH_4)$ to $Cp^*Re(CO)_2(CH_3)H$ as an equilibrium mixture ($k = (5 \pm 2) \times 10^8$ s^{-1}). Finally, these species react back with CO to $Cp^*Re(CO)_3$ over hundreds of microseconds. The position of equilibrium shifts toward the alkane complex with the Cp analogue and with use of ethane instead of methane. The spectra show very conspicuously that the ν(CO) bands of the Re(I) complexes lie *ca.* 50 cm^{-1} to high frequency of the isomeric Re(II) complexes.

The formation of labile metal alkyl hydrides carries implications for the mechanisms of synthesis of stable products in hydrocarbon solution formed by oxidative addition, substitution or by formation of dinuclear products. All these processes require the intermediacy of metal alkyl hydrides in alkanes or metal aryl hydrides in arenes. Nowhere is this more conspicuous than in the cases of $CpRh(CO)_2$ and $Cp^*Rh(CO)_2$. The initial stage is, as usual, immediate CO loss and formation of an alkane complex that then converts to the alkyl hydride complex. The reactions have been studied in liq Kr at low temperature[176] and in liquid or supercritical alkanes[177] at room temperature. The lifetime of linear alkane complexes is in the range 3-18 ns at room temperature and varies systematically with the length of the alkane chain as a consequence of subtle interplay between 1,2-shifts of the metal along the chain (chain walking) and oxidative cleavage of the primary C–H bond.[176] Complexes of cyclic alkanes undergo oxidative cleavage more slowly than their linear counterparts.

Flash photolysis and TRIR spectroscopy in combination with matrix isolation demonstrated what happens next. The CpRh(CO)(cyclohexyl)H now acts as a long-lived store of the unsaturated intermediate.[178] In the absence of other ligands, the symmetrical dimer $[CpRh(\mu\text{-}CO)]_2$ is formed over tens of milliseconds. The latter reacts with CO to yield the final stable product $[CpRh(CO)]_2(\mu\text{-}CO)$ ($k = (1.2 \pm 0.1) \times 10^3$ dm^3 mol^{-1} s^{-1}). The structure of $[CpRh(\mu\text{-}CO)]_2$ was proved by polarised photochemistry in matrices. In the presence of added silane, Et_3SiH, the CpRh(CO)(cyclohexyl)H reacts to form $CpRh(CO)(SiEt_3)H$ by complex kinetics‖ with a limiting rate at high $[Et_3SiH]$ of 2.7×10^3 s^{-1}.[178]

Applications to synthesis of complexes with labile ligands: key points

(1) Labile ligands act as stores of reaction intermediates.
(2) Matrix isolation, time-resolved spectroscopy and photolysis in liq and sc noble gases enable characterisation of metal carbonyl complexes with η^2-H_2, N_2, alkane, noble-gas and silane ligands.
(3) Kinetics of formation and their onward reactivity have been determined.
(4) For some precursors, reaction with alkanes to form C–H oxidative addition products occurs within 2 ps of the initial laser pulse. For others, it is possible to detect alkane complexes as precursors to oxidative addition.
(5) The C–H oxidative addition products may themselves be very labile.

‖ The quantum yield for formation of $CpRh(CO)(SiEt_3)H$ from $CpRh(CO)_2$ is independent of $[Et_3SiH]$ as expected, but the quantum yield for photosubstitution of $CpRh(CO)_2$ by PPh_3 is dependent on $[PPh_3]$ implying that there is also another mechanism, probably a ring-slipped intermediate. The quantum yields for both reactions are strongly wavelength dependent. Dunwoody and Lees, *Organometallics*, 1997, **16**, 5770.

7. Photocatalysis

In a recent review on metal hydride photochemistry, Perutz and Procacci[162] described the different types of photocatalysis following Wrighton[1] and Hennig.[179] The quantum yield, ϕ, is often the key measurement that distinguishes photoinduced catalysis from photoassisted catalysis. In the former, the photochemical act lies outside the catalytic cycle which consists of thermal reactions, ϕ may be greater than unity and the free energy of the catalytic reaction must be negative. In photoassisted catalysis, the photochemical act lies inside the cycle and $\phi \leq 1$, but the free energy may be positive. Photocatalysis may be achieved with the aid of a photosensitiser, though this is uncommon for metal carbonyls. Photosensitised catalysis requires transfer of either an electron or excitation energy from the sensitiser to an acceptor and can belong to either of the above classes.

One early example of C–H activation of alkanes stands out. Goldman and colleagues observed catalytic dehydrogenation of cycloalkanes with $Rh(PMe_3)_2(CO)Cl$ (0.1%) as photocatalyst with turnover numbers up to 5000 for cyclooctane. The quantum yield is inversely dependent on the pressure of added CO and independent of pressure of added H_2.[180] There is a large kinetic isotope effect when using cyclohexane and its deuterated analogues. Considering also that the free energy for this reaction is positive, this must be photoassisted catalysis. The evidence indicates that this reaction is driven by photochemical CO loss within the catalytic cycle, followed by alkane oxidative addition.[180] That $Rh(PMe_3)_2(CO)Cl$ undergoes photochemical CO loss has been confirmed by nanosecond TRIR.[181] Time-resolved absorption suggests that there may be an excited state[181] with time-constant *ca.* 40 ps preceding CO loss, but ultrafast IR data are lacking. Beller and colleagues have revisited this reaction and improved the conditions so that linear alkanes can also be dehydrogenated with good turnover numbers.[182] With the benefit of DFT calculations and a thermodynamic cycle, their results indicate that reaction of the CO-loss product $RhCl(PMe_3)_2$ with octane is likely to be uphill. They therefore suggest that the reaction occurs from an excited state of $Rh(PMe_3)_2(CO)Cl$, but they did not explain the CO inhibition of the quantum yield.

The borylation of linear alkanes is a reaction with negative free energy and therefore could proceed by either photoassisted or photoinduced catalysis. Hartwig and colleagues demonstrated that $Cp^*Re(CO)_3$ (2.5%) under CO (2 bar) reacts photocatalytically with pentane and B_2pin_2 (pin = pinacolate) to form RBpin (R = pentyl) in 95% yield with respect to B_2pin_2 (*i.e.* 38 turnovers). The dicarbonyl $Cp^*Re(CO)_2(Bpin)_2$ (mixture of *cis* and *trans* isomers) was isolated from the reaction and also acted as a photocatalyst, presumably *via* photochemical CO loss.[183] More recently, $CpFe(CO)_2(Cu(IPr))$ (IPr = *N*,*N*′-bis(2,6- diisopropylphenyl)imidazol-2-ylidene) has been used as the photocatalyst for arene borylation by HBpin. The catalytic cycle is postulated to involve formation of Cu(IPr)H and $CpFe(CO)_2(Bpin)$ which reacts photochemically with arene to form $CpFe(CO)_2H$ and Ar(Bpin).[184] Similar photocatalytic reactions have been performed with $Rh(PMe_3)_2(CO)Cl$ as photocatalyst, this time with the suggestion of CO photodissociation outside the cycle, *i.e.* photoinduced catalysis – surprising considering the alkane dehydrogenation.[185]

One of the most spectacular examples of photoinduced catalysis is the reaction of $CpWH(CO)_3$ which undergoes CO substitution by PBu_3 on UV irradiation *via* a radical chain reaction started by W–H homolysis ($\phi > 30$). In the presence of small quantities of $[CpW(CO)_3]_2$, the quantum yield increased to about 1000.[186] This reaction exploits the ability of metal hydride carbonyls to undergo photochemical homolysis of the M–H bond and the rapid thermal substitution of 17-electron species.

Photochemical reactions can also be used to identify short-lived intermediates in thermal catalytic reactions as exemplified in Scheme 3. Photochemical initiation benefits mechanistic investigation because the commencement of reaction is synchronised allowing the reaction sequence to be monitored at times from picoseconds to milliseconds in and beyond.

The mechanism of photocatalytic hydrogenation of norbornadiene by chromium carbonyls is considered in Section 6.3. Manganese and iron carbonyls continue to be used as photocatalysts for hydrosilation of ketones, aldehydes and carboxylic acids.[187]

Photocatalysis: key points

(1) Catalytic reactions initiated by photochemical processes, *e.g.* ligand dissociation.

(2) Photoinduced catalysis: light absorption outside catalytic cycle, ϕ unlimited, $\Delta G_{reaction}$ negative.

(3) Photoassisted catalysis: light absorption inside catalytic cycle, $\phi \leq 1$, $\Delta G_{reaction}$ positive or negative.

8. Conclusions and outlook

In this Tutorial Review, we have probed the subtlety of the photochemistry of transition metal carbonyls, emphasising the behaviour of the intermediates. We have shown the importance of metal carbonyl photochemistry to understanding fundamental principles of transition-metal chemistry and photochemistry, as well as to applications such as photocatalysis. In describing these results, we have delved into state-of-the art techniques, especially those of time-resolved spectroscopy. The principles that we have developed in each section have been summarised in text-boxes. The most important of these conclusions are brought together as Key Learning Points at the start of this review.

Abbreviations

CASSCF	Complete active space self-consistent field
CCSD(T)	Coupled-cluster with single and double and perturbative triple excitations
CORM	Carbon monoxide releasing molecule
DFT	Density functional theory
EFFF	Energy factored force field
EPR	Electron paramagnetic resonance

FTIR	Fourier transform infrared
IR	Infrared
MLCT	Metal-to-ligand charge transfer
Ng	Noble gas
NMR	Nuclear magnetic resonance
PFMCH	Perfluoromethylcyclohexane
PhotoCORM	Photochemical carbon monoxide releasing molecule
RIXS	Resonant inelastic X-ray scattering
sc	supercritical
THF	Tetrahydrofuran
TRIR	Time-resolved infrared
UV	Ultraviolet
XAFS	X-ray absorption fine structure
XANES	X-ray absorption near-edge structure

Conflicts of interest

There are no conflicts of interest to declare.

Acknowledgements

We thank all of our colleagues, students and coworkers who have contributed to the work described in this Review. We are grateful to the funders who have supported our work and to the generations of skilled technicians who built the equipment needed to perform our research.

References

1 M. S. Wrighton, *Chem. Rev.*, 1974, **74**, 401–430.
2 R. N. Perutz, O. Torres and A. Vlček, Jr., in *Comprehensive Inorganic Chemistry II*, ed. J. Reedijk and K. Poeppelmeier, Elsevier, Oxford, 2013, vol. 8, ch. 8.06, pp. 229–253.
3 H. Braunschweig, R. D. Dewhurst, K. Radacki, C. W. Tate and A. Vargas, *Angew. Chem., Int. Ed.*, 2014, **53**, 6263–6266.
4 J. D. Watson, L. D. Field and G. E. Ball, *Nat. Chem.*, 2022, DOI: **10.1038/s41557-022-00929-w**.
5 B. E. Mann, *Organometallics*, 2012, **31**, 5728–5735.
6 P. C. Ford, *Coord. Chem. Rev.*, 2018, **376**, 548–564.
7 Z. Li, A. E. Pierri, P.-J. Huang, G. Wu, A. V. Iretskii and P. C. Ford, *Inorg. Chem.*, 2017, **56**, 6094–6104.
8 R. Sakla, A. Singh, R. Kaushik, P. Kamur and D. A. Jose, *Inorg. Chem.*, 2019, **58**, 10761–10768.
9 S. H. C. Askes, G. U. Reddy, R. Wyrwa, S. Bonnet and A. Schiller, *J. Am. Chem. Soc.*, 2017, **139**, 15292–15295.
10 L. A. Hammarback, B. J. Aucott, J. T. W. Bray, I. P. Clark, M. Towrie, A. Robinson, I. J. S. Fairlamb and J. M. Lynam, *J. Am. Chem. Soc.*, 2021, **143**, 1356–1364.
11 C. P. Simpson, O. L. Adebolu, J.-S. Kim, V. Vasu and A. D. Asandei, *Macromolecules*, 2015, **48**, 6404–6420.
12 M. Chen, A. Pekker, W. Li, M. E. Itkis, R. C. Haddon and E. Bekyarova, *Carbon*, 2018, **129**, 450–455.
13 E. G. Look and H. D. Gafney, *J. Phys. Chem., C*, 2013, **117**, 12268–12279.
14 For a review of bandwidths, see J. J. Turner, in *Handbook of Vibrational Spectroscopy*, ed. J. M. Chalmers and P. R. Griffiths, J. Wiley, Chichester, UK, 2002, vol. 1, pp. 101–127.
15 W. B. Maier II, M. Poliakoff, M. B. Simpson and J. J. Turner, *J. Chem. Soc., Chem. Commun.*, 1980, 587–589.
16 S. J. Barlow, M. W. George and M. Poliakoff, in *Handbook of vibrational spectroscopy*, ed. J. M. Chalmers and P. R. Griffiths, J. Wiley, Chichester, UK, 2002, vol. 4, pp. 3124–3136.
17 C. S. Kraihanzel and F. A. Cotton, *Inorg. Chem.*, 1963, **2**, 533–540 and references therein.
18 For an excellent overall picture of metal carbonyl spectra, see P. S. Braterman, *Metal Carbonyl Spectra*, Academic Press, London, 1975.
19 L. H. Jones, *Inorganic Vibrational Spectroscopy*, Marcell Dekker, New York, 1971.
20 J. K. Burdett, R. N. Perutz, M. Poliakoff and J. J. Turner, *Inorg. Chem.*, 1976, **15**, 1245.
21 J. K. Burdett, M. Poliakoff, J. A. Timney and J. J. Turner, *Inorg. Chem.*, 1978, **17**, 948–952.
22 C. A. Tolman, *J. Am. Chem. Soc.*, 1970, **92**, 2953–2956.
23 D. G. Gusev, *Organometallics*, 2009, **28**, 763–770.
24 R. K. Hocking and T. W. Hambley, *Organometallics*, 2007, **26**, 2815–2823.
25 J. A. Timney, *Inorg. Chem.*, 1979, **18**, 2502.
26 J. A. Timney, *Spectrochim. Acta, Part A*, 1995, **53**, 33–38.
27 D. C. Grills and M. W. George, in *Handbook of Vibrational Spectroscopy*, ed. J. M. Chalmers and P. R. Griffiths, J. Wiley, Chichester, UK, 2002, vol. 1, pp. 677–693.
28 H. Hermann, F.-W. Grevels, A. Henne and K. Schaffner, *J. Phys. Chem.*, 1982, **86**, 5151–5154.
29 E. R. Kennehan, K. T. Munson, C. Grieco, G. S. Doucette, A. R. Marshall, M. C. Beard and J. B. Asbury, *J. Am. Chem. Soc.*, 2021, **143**, 13824–13834.
30 R. N. Sampaio, D. C. Grills, D. E. Polyansky, D. J. Szalda and E. Fujita, *J. Am. Chem. Soc.*, 2020, **142**, 2413–2428.
31 P. Portius, J. Yang, X.-Z. Sun, D. C. Grills, P. Matousek, A. W. Parker, M. Towrie and M. W. George, *J. Am. Chem. Soc.*, 2004, **126**, 10713–10720.
32 M. K. Kuimova, W. Z. Alsindi, J. Dyer, D. C. Grills, O. S. Jina, P. Matousek, A. W. Parker, P. Portius, X. Z. Sun, M. Towrie, C. Wilson, J. Yang and M. W. George, *Dalton Trans.*, 2003, 3996–4006.
33 X. Wu, Z. Liu, T. S. Murphy, X. Z. Sun, M. W.-D. Hanson-Heine, M. Towrie, J. N. Harvey and M. W. George, *Faraday Discussions*, 2019, **220**, 86–104.
34 I. W. Stolz, G. R. Dobson and R. K. Sheline, *J. Am. Chem. Soc.*, 1962, **84**, 3589–3590.
35 I. W. Stolz, G. R. Dobson and R. K. Sheline, *J. Am. Chem. Soc.*, 1963, **85**, 1013–1014.
36 See, e.g.: H. W. Brown and G. C. Pimentel, *J. Chem. Phys.*, 1958, **29**, 883–888.
37 A. J. Rest and J. J. Turner, *J. Chem. Soc. D: Chem. Commun.*, 1969, 375–376.
38 M. A. Graham, M. Poliakoff and J. J. Turner, *J. Chem. Soc. A*, 1971, 2939–2948.

39 R. N. Perutz and J. J. Turner, *Inorg. Chem.*, 1975, **14**, 262–270.
40 R. N. Perutz and J. J. Turner, *J. Am. Chem. Soc.*, 1975, **97**, 4791–4799.
41 J. K. Burdett, J. M. Grzybowski, R. N. Perutz, M. Poliakoff, J. J. Turner and R. F. Turner, *Inorg. Chem.*, 1978, **17**, 147–154.
42 J. J. Turner, J. K. Burdett, R. N. Perutz and M. Poliakoff, *Pure Appl. Chem.*, 1977, **49**, 271–285.
43 J. Nasielski and A. Colas, *J. Organomet. Chem.*, 1975, **101**, 215–219.
44 M. Poliakoff, *Inorg. Chem.*, 1976, **15**, 2022–2031.
45 M. Poliakoff, *Inorg. Chem.*, 1976, **15**, 2892–2897.
46 R. N. Perutz and J. J. Turner, *J. Am. Chem. Soc.*, 1975, **97**, 4800–4804.
47 M. J. Almond, J. A. Crayston, A. J. Downs, M. Poliakoff and J. J. Turner, *Inorg. Chem.*, 1986, **25**, 19–25.
48 M. Zhou, L. Andrews and C. W. Bauschlicher, *Chem. Rev.*, 2001, **101**, 1931–1961.
49 X. Wu, L. Zhao, J. Jin, S. Pan, P. Sudip, W. Li, J. Xiaoyang, W. Guanjun, Z. Mingfei and G. Frenking, *Science*, 2018, **361**, 912–916.
50 M. Poliakoff and J. J. Turner, *J. Chem. Soc., Dalton Trans.*, 1973, 1351–1357.
51 M. Poliakoff and J. J. Turner, *J. Chem. Soc., Dalton Trans.*, 1974, 2275–2285.
52 M. Poliakoff and J. J. Turner, *Angew. Chem., Int. Ed.*, 2001, **40**, 2809–2812.
53 T. J. Barton, R. Grinter, A. J. Thomson, B. Davies and M. Poliakoff, *J. Chem. Soc., Chem. Commun.*, 1977, 841–842.
54 M. Poliakoff and E. Weitz, *Acc. Chem. Res.*, 1987, **20**, 408–414.
55 H. Ihee, J. Cao and A. H. Zewail, *Chem. Phys. Lett.*, 1997, **281**, 10–19.
56 H. Ihee, J. Cao and A. H. Zewail, *Angew. Chem., Int. Ed.*, 2001, **40**, 1532–1535.
57 M. Poliakoff, *J. Chem. Soc., Dalton Trans.*, 1974, 210–212.
58 C. R. Kemnitz, E. S. Ball and R. J. McMahon, *Organometallics*, 2012, **31**, 70–84.
59 T. J. Meyer and J. V. Caspar, *Chem. Rev.*, 1985, **85**, 187–218.
60 A. F. Hepp and M. S. Wrighton, *J. Am. Chem. Soc.*, 1983, **105**, 5934–5935.
61 I. R. Dunkin, P. Harter and C. J. Shields, *J. Am. Chem. Soc.*, 1984, **106**, 7248–7249.
62 S. P. Church, M. Poliakoff, J. A. Timney and J. J. Turner, *J. Am. Chem. Soc.*, 1981, **103**, 7515–7520.
63 S. A. Fairhurst, J. R. Morton, R. N. Perutz and K. F. Preston, *Organometallics*, 1984, **3**, 1389–1391.
64 R. H. Hooker, K. A. Mahmoud and A. J. Rest, *J. Chem. Soc. Chem. Commun.*, 1983, 1022–1024.
65 A. F. Hepp, J. P. Blaha, C. Lewis and M. S. Wrighton, *Organometallics*, 1984, **3**, 174–177.
66 J. P. Blaha, B. E. Bursten, J. C. Dewan, R. B. Frankel, C. L. Randolph, B. A. Wilson and M. S. Wrighton, *J. Am. Chem Soc.*, 1985, **107**, 4561–4562.
67 F. A. Kvietok and B. E. Bursten, *J. Am. Chem. Soc.*, 1994, **116**, 9807–9808.
68 G. Nathanson, B. Gitlin, A. M. Rosan and J. T. Yardley, *J. Chem. Phys.*, 1981, **74**, 361–370.
69 A. J. Ouderkirk, P. Werner, N. L. Schultz and E. Weitz, *J. Am. Chem. Soc.*, 1983, **105**, 3354–3355.
70 K. Tanaka, Y. Tachikawa, K. Sakaguchi, T. Hikida and T. Tanaka, *J. Chem. Phys.*, 1999, **111**, 3970–3977 and references therein.
71 E. Weitz, *J. Phys. Chem.*, 1994, **98**, 11256–11264.
72 T. A. Seder, S. P. Church and E. Weitz, *J. Am. Chem. Soc.*, 1986, **108**, 7518–7524.
73 R. Cercola, K. C. Fischer, S. L. Sherman, E. Garans, N. G.-K. Wong, L. A. Hammerback, J. M. Lynam, I. J. S. Fairlamb and C. Dessent, *Chem. – Eur. J.*, 2020, **26**, 10297–10306.
74 A. B. Wolk, C. M. Leavitt, E. Garand and M. A. Johnson, *Acc. Chem. Res.*, 2014, **47**, 202–210.
75 B. J. Aucott, J. B. Eastwood, L. A. Hammerback, I. P. Clark, I. V. Sazanovich, M. Towrie, I. J. S. Fairlamb and J. M. Lynam, *Dalton Trans.*, 2019, **48**, 16426–16436.
76 P. Wernet, T. Leitner, I. Josefsson, T. Mazza, P. S. Miedema, H. Schröder, M. Beye, K. Kunnus, S. Schreck, P. Radcliffe, S. Düsterer, M. Meyer, M. Odelius and A. Föhlisch, *J. Chem. Phys.*, 2017, **146**, 211103.
77 T. Leitner, I. Josefsson, T. Mazza, P. S. Miedema, H. Schröder, M. Beye, K. Kunnus, S. Schreck, S. Düsterer, A. Föhlisch, M. Meyer, M. Odelius and P. Wernet, *J. Chem. Phys.*, 2018, **149**, 044307.
78 J. M. Kelly, H. Hermann and E. K. von Gustorf, *J. Chem. Soc., Chem. Commun.*, 1973, 105–106.
79 S. P. Church, F.-W. Grevels, H. Hermann and K. Schaffner, *Inorg. Chem.*, 1985, **24**, 418–422.
80 R. Bonneau and J. M. Kelly, *J. Am. Chem. Soc.*, 1980, **102**, 1220–1221.
81 L. Biber, D. Reuvenov, T. Revzin, T. Sinai, A. Zahavi and R. H. Schultz, *Dalton Trans.*, 2007, 41–51.
82 A. A. Bengali and T. F. Stumbaugh, *Dalton Trans.*, 2003, 354–360.
83 A. G. Joly and K. A. Nelson, *J. Phys. Chem.*, 1989, **93**, 2876–2878.
84 T. P. Dougherty and E. J. Heilweil, *Chem. Phys. Lett.*, 1994, **227**, 19–25.
85 S. M. Arrivo, T. P. Dougherty, W. T. Grubbs and E. J. Heilweil, *Chem. Phys. Lett.*, 1995, **235**, 247–254.
86 T. Lian, S. E. Bromberg, M. C. Asplund, H. Yang and C. B. Harris, *J. Phys. Chem.*, 1996, **100**, 11994–12001.
87 J. E. Shanoski, E. A. Glascoe and C. B. Harris, *J. Phys. Chem. B*, 2006, **110**, 996–1005.
88 S. P. Church, H. Hermann, F.-W. Grevels and K. Schaffner, *J. Chem. Soc., Chem. Commun.*, 1984, 785–786.
89 J. Z. Zhang and C. B. Harris, *J. Chem. Phys.*, 1991, **95**, 4024–4032.
90 B. D. Moore, M. B. Simpson, M. Poliakoff and J. J. Turner, *J. Chem. Soc., Chem. Commun.*, 1984, 972–974.
91 C. M. Brookes, J. P. Lamont, S. C. Nguyen, J. A. Calladine, X.-Z. Sun, C. B. Harris and M. W. George, *Polyhedron*, 2014, **72**, 130–134 and references therein.
92 A. J. Dixon, M. A. Healy, M. Poliakoff and J. J. Turner, *J. Chem. Soc, Chem. Commun.*, 1986, 994–996.

93 C. J. Arnold, T.-Q. Ye, R. N. Perutz, R. E. Hester and J. N. Moore, *Chem. Phys. Lett.*, 1996, **248**, 464–469.
94 M. B. Simpson, M. Poliakoff, J. J. Turner, W. B. Maier Il and J. G. McLaughlin, *J. Chem. Soc., Chem. Commun.*, 1983, 1355–1357.
95 B. H. Weiller, *J. Am. Chem. Soc.*, 2002, **114**, 10910–10915.
96 X.-Z. Sun, M. W. George, S. G. Kazarian, S. M. Nikiforov and M. Poliakoff, *J. Am. Chem. Soc.*, 1996, **118**, 10525–10532.
97 M. Besora, J.-L. Carreón-Macedo, A. J. Cowan, M. W. George, J. N. Harvey, P. Portius, K. L. Ronayne, X.-Z. Sun and M. Towrie, *J. Am. Chem. Soc.*, 2009, **131**, 3583–3592.
98 V. Bachler, F.-W. Grevels, K. Kerpen, G. Olbrich and K. Schaffner, *Organometallics*, 2003, **22**, 1696–1711.
99 P. T. Snee, C. K. Payne, K. T. Kotz, H. Yang and C. B. Harris, *J. Am. Chem. Soc.*, 2001, **123**, 2255–2264.
100 H. Yang, M. C. Asplund, K. T. Kotz, M. J. Wilkens, H. Frei and C. B. Harris, *J. Am. Chem. Soc.*, 1998, **120**, 10154–10165.
101 J. W. Kee, Y. Y. Tan, B. H.-G. Swennenhuis, A. A. Bengali and W. Y. Fan, *Organometallics*, 2011, **30**, 2154–2159.
102 X.-Z. Sun, D. C. Grills, S. M. Nikiforov, M. Poliakoff and M. W. George, *J. Am. Chem. Soc.*, 1997, **119**, 7521.
103 S. Geftakis and G. E. Ball, *J. Am. Chem. Soc.*, 1998, **120**, 9953–9954.
104 J. A. Calladine, S. B. Duckett, M. W. George, S. L. Matthews, R. N. Perutz, O. Torres and K. Q. Vuong, *J. Am. Chem. Soc.*, 2011, **133**, 2303–2310.
105 W. H. Bernskoetter, C. K. Schauer, K. I. Goldberg and M. Brookhart, *Science*, 2009, **326**, 553–556.
106 G. E. Ball, T. A. Darwish, S. Geftakis, M. W. George, D. J. Lawes, P. Portius and J. P. Rourke, *Proc. Nat. Acad. Sci. U. S. A.*, 2005, **102**, 1853–1858.
107 P. Wernet, K. Kunuus, I. Josefsson, I. Rajkovic, W. Quevedo, M. Beye, S. Schreck, S. Grübel, M. Scholz, D. Nordlund, W. Zhang, R. W. Hartsock, W. F. Schlotter, J. J. Turner, B. Kennedy, F. Hennies, F. M.-F. de Groot, K. J. Gaffney, S. Techert, M. Odelius and A. Föhlisch, *Nature*, 2015, **520**, 78–81.
108 K. Kunnus, I. Josefsson, I. Rajkovic, S. Schreck, W. Quevedo, M. Beye, C. Weniger, S. Grübel, M. Scholz, D. Nordlund, W. Zhang, R. W. Hartsock, K. J. Gaffney, W. F. Schlotter, J. J. Turner, B. Kennedy, F. Hennies, F. M.-F. de Groot, S. Techert, M. Odelius, P. Wernet and A. Föhlisch, *Struct. Dyn.*, 2016, **3**, 043204.
109 H. Cho, K. Hong, M. L. Strader, J. H. Lee, R. W. Schoellein, N. Huse and T. K. Kim, *Inorg. Chem.*, 2016, **55**, 5895–5903.
110 S. A. Bartlett, N. A. Besley, A. J. Dent, S. Diaz-Moreno, J. Evans, M. L. Hamilton, M. W.-D. Hanson-Heine, R. L. Horvath, V. Manici, X.-Z. Sun, M. Towrie, L. Wu, X. Zhang and M. W. George, *J. Am. Chem. Soc.*, 2019, **141**, 11471–11480.
111 A. S. Weller, F. M. Chadwick and A. I. Mckay, *Adv. Organomet. Chem.*, 2016, **66**, 223–276.
112 R. H. Crabtree, *Struct. Bond.*, 2017, **171**, 63–77.
113 J. K. Burdett, *J. Chem. Soc., Faraday Trans. 2*, 1974, **70**, 1599–1613.
114 M. Elian and R. Hoffmann, *Inorg. Chem.*, 1975, **14**, 1059–1076.
115 J. K. Burdett, *Inorg. Chem.*, 1975, **14**, 375–382.
116 A. R. Rossi and R. Hoffmann, *Inorg. Chem.*, 1975, **14**, 365–374.
117 P. Portius, M. Bühl, M. W. George, F.-W. Grevels and J. J. Turner, *Organometallics*, 2019, **38**, 4288–4297.
118 J. H. Jang, J. G. Lee, H. Lee, Y. Xie and H. F. Schaefer III, *J. Phys. Chem. A*, 1998, **102**, 5298–5304.
119 Obtained by, among other techniques, the vacuum UV photolysis of $Cr(CO)_6$ in low-temperature matrices: P. A. Breeze, J. K. Burdett and J. J. Turner, *Inorg. Chem.*, 1981, **20**, 3369–3378.
120 See J. Kim, J. Kim and H. Ihee, *J. Phys. Chem. A*, 2013, **117**, 3861–3868 for some relevant references.
121 Z. Sun, H. F. Schaefer III, Y. Xie, Y. Liu and R. Zhong, *J. Comput. Chem.*, 2014, **35**, 998–1009.
122 For example: On $Cr(CO)_6/Cr(CO)_5$; L. A. Barnes, L. Bowen and R. Lindh, *J. Chem. Phys.*, 1993, **98**, 3978–3989; A. W. Ehlers and G. Frenking, *J. Am. Chem. Soc.*, 1994, **116**, 1514–1520.
123 On $Fe(CO)_5/Fe(CO)_4$; L. A. Barnes, M. Rosi and C. W. Bauschlicher, Jr., *J. Chem. Phys.*, 1991, **94**, 2031–2039.
124 J. Kim, T. K. Kim, J. Kim, Y. S. Lee and H. Ihee, *J. Phys. Chem. A*, 2007, **111**, 4697–4710.
125 T. Witte, J. S. Yeston, M. Motzkus, E. J. Heilweil and K.-L. Kompa, *Chem. Phys. Lett.*, 2004, **392**, 156–161.
126 C. R. Baiz, P.-l McRobbie, J. M. Anna, E. Geva and K. J. Kubarych, *Acc. Chem. Res.*, 2009, **42**, 1395–1404.
127 A. W. Ehlers, G. Frenking and E. J. Baerends, *Organometallics*, 1997, **16**, 4896–4902.
128 A. Rosa, E. J. Baerends, S. J.-A. van Gisbergen, E. van Lenthe, J. A. Groeneveld and J. G. Snijders, *J. Am. Chem. Soc.*, 1999, **121**, 10356–10365.
129 S. Villaume, A. Strich, C. Daniel, S. A. Perera and R. J. Bartlett, *Phys. Chem. Chem. Phys.*, 2007, **9**, 6115.
130 P. Hummel, J. Oxgaard, W. A. Goddard, III and H. B. Gray, *Inorg. Chem.*, 2005, **44**, 2454.
131 S. A. Trushin, K. Kosma, W. Fuss and W. E. Schmid, *Chem. Phys.*, 2008, **347**, 309–323. This paper also provides references to the appropriate UV/Vis studies, and also earlier similar work.
132 M. J. Paterson, P. A. Hunt, M. A. Robb and O. Takahashi, *J. Phys. Chem. A*, 2002, **106**, 10494–10504.
133 T. P.-M. Goumans, A. W. Ehlers, M. C. van Hemert, A. Rosa, E.-J. Baerends and K. Lammertsma, *J. Am. Chem. Soc.*, 2003, **125**, 3558–3567.
134 B. Davies, A. McNeish, M. Poliakoff and J. J. Turner, *J. Am. Chem. Soc.*, 1977, **99**, 7573–7579.
135 M. Poliakoff and A. Ceulemans, *J. Am. Chem. Soc.*, 1984, **106**, 50–54.
136 S. A. Trushin, W. Fuss, K. L. Kompa and W. E. Schmid, *J. Phys. Chem. A*, 2000, **104**, 1997–2006.
137 R. J. Ryther and E. Weitz, *J. Phys. Chem.*, 1992, **96**, 2561–2567.
138 M. Besora, J. Carreón-Macedo, A. Cimas and J. N. Harvey, *Adv. Inorg. Chem.*, 2009, **61**, 573–623.
139 T. Takayanagi, Y. Watabe and T. Miyazaki, *Molecules*, 2020, **25**, 882–891.

140 M. C. Heitz and C. Daniel, *J. Am Chem. Soc.*, 1997, **119**, 8269–8275.
141 A. Rosa, G. Ricciardi, E. J. Baerends and D. J. Stufkens, *Inorg. Chem.*, 1995, **34**, 3425–3432.
142 M. P. Wilms, E. J. Baerends, A. Rosa and D. J. Baerends, *Inorg. Chem.*, 1997, **36**, 1541–1551.
143 I. P. Clark, M. W. George, G. M. Greetham, E. C. Harvey, C. Long, J. C. Manton and M. T. Pryce, *J. Phys. Chem. A*, 2011, **115**, 2985–2993.
144 M. W. George, C. Long, M. T. Pryce, X. Z. Sun and K. Q. Vuong, *Organometallics*, 2012, **31**, 268–272 and references therein.
145 B. Procacci, S. B. Duckett, M. W. George, M. W.-D. Hanson-Heine, R. Horvath, R. N. Perutz, X. Z. Sun, K. Q. Vuong and J. A. Welch, *Organometallics*, 2018, **37**, 855–868 and references therein.
146 P. Glyn, M. W. George, P. M. Hodges and J. J. Turner, *J. Chem. Soc., Chem. Commun.*, 1989, 1655–1657.
147 J. M. Butler, M. W. George, J. R. Schoonover, D. M. Dattelbaum and T. J. Meyer, *Coord. Chem. Rev.*, 2007, **251**, 492–514.
148 C. D. Windle, M. W. George, R. N. Perutz, P. A. Summers, X. Z. Sun and A. C. Whitwood, *Chem. Sci*, 2015, **5**, 6847–6854.
149 M. Pižl, A. Picchiotti, M. Rebarz, N. Lenngren, L. Yingliang, S. Záliš, M. Kloz and A. Vlček, *J. Phys. Chem. A*, 2020, **124**, 1253–1265.
150 A. El Nahhas, R. M. van der Veen, T. J. Penfold, V. T. Pham, F. A. Lima, R. Abela, A. M. Blanco-Rodriguez, S. Zalis, A. Vlcek, I. Tavernelli, U. Rothlisberger, C. J. Milne and M. Chergui, *J. Phys. Chem. A*, 2013, **117**, 361–369.
151 R. N. Perutz, S. Sabo-Etienne and A. S. Weller, *Angew. Chem., Int. Ed.*, 2022, **134**, e202111462 and references therein.
152 A. D. Allen and C. V. Senoff, *Chem. Commun.*, 1965, 621–622.
153 A. J. Rest, *J. Organomet. Chem.*, 1972, **40**, C76–C78.
154 J. J. Turner, M. B. Simpson, M. Poliakoff and W. B. Maier II, *J. Am. Chem. Soc.*, 1983, **105**, 3898–3904.
155 J. J. Turner, M. B. Simpson, M. Poliakoff, W. B. Maier II and M. A. Graham, *Inorg. Chem.*, 1983, **22**, 911–920.
156 S. P. Church, F.-W. Grevels, H. Hermann and K. Schaffner, *Inorg. Chem.*, 1984, **23**, 3830–3833.
157 E. F. Walsh, V. K. Popov, M. W. George and M. Poliakoff, *J. Phys. Chem.*, 1995, **99**, 12016–12020.
158 See *e.g.*, D. C. Grills, K.-W. Huang, J. T. Muckerman and E. Fujita, *Coord. Chem. Rev.*, 2006, **250**, 1681–1695, and references therein.
159 J. B. Eastwood, L. A. Hammarback, M. T. McRobie, I. P. Clark, M. Towrie, I. J.-S. Fairlamb and J. M. Lynam, *Dalton Trans.*, 2020, **49**, 5463–5470.
160 G. J. Kubas, *Chem. Rev.*, 2007, **107**, 4152–4205.
161 R. H. Crabtree, *Chem. Rev.*, 2016, **116**, 8750–8769.
162 R. N. Perutz and B. Procacci, *Chem. Rev.*, 2016, **116**, 8506–8544.
163 R. L. Sweany, *J. Am. Chem. Soc.*, 1985, **107**, 2374–2379.
164 R. K. Upmacis, M. Poliakoff and J. J. Turner, *J. Am. Chem. Soc.*, 1986, **108**, 3645–3651.
165 S. P. Church, F.-W. Grevels, H. Hermann and K. Schaffner, *J. Chem. Soc., Chem. Commun.*, 1985, 30–32.
166 S. L. Matthews and D. M. Heinekey, *J. Am. Chem. Soc.*, 2006, **128**, 2615–2620.
167 P. M. Hodges, S. A. Jackson, J. Jacke, M. Poliakoff, J. J. Turner and F.-W. Grevels, *J. Am. Chem. Soc.*, 1990, **112**, 1234–1244 and references therein.
168 M. T. Haward, M. W. George, P. Hamley and M. Poliakoff, *J. Chem. Soc., Chem. Commun.*, 1991, 1101–1103.
169 A. H. Janowicz and R. G. Bergman, *J. Am. Chem. Soc.*, 1982, **104**, 352–354.
170 J. K. Hoyano and W. A. G. Graham, *J. Am. Chem. Soc.*, 1982, **104**, 3723–3725.
171 J. K. Hoyano, A. D. McMaster and W. A. G. Graham, *J. Am. Chem. Soc.*, 1983, **105**, 7190–7191.
172 A. J. Rest, I. Whitwell, W. A. G. Graham, J. K. Hoyano and A. D. McMaster, *J. Chem. Soc., Dalton Trans.*, 1987, 1181–1190and references therein.
173 P. E. Bloyce, A. J. Rest, I. Whitwell, W. A. G. Graham and R. Holmes-Smith, *J. Chem. Soc. Chem. Commun.*, 1988, 846–848.
174 J. B. Asbury, K. Hang, J. S. Yeston, J. G. Cordaro, R. G. Bergman and T. Lian, *J. Am. Chem. Soc.*, 2000, **122**, 12870–12871.
175 A. J. Cowan, P. Portius, H. K. Kawanami, O. S. Jina, D. C. Grills, X.-Z. Sun, J. McMaster and M. W. George, *Proc. Natl. Acad. Sci. U. S. A.*, 2007, **104**, 6933–6938.
176 B. K. McNamara, J. S. Yeston, R. G. Bergman and C. B. Moore, *J. Am. Chem. Soc.*, 1999, **121**, 6437–6443.
177 M. W. George, M. B. Hall, O. S. Jina, P. Portius, X.-Z. Sun, M. Towrie, H. Wu, X. Yang and S. D. Zarić, *Proc. Natl. Acad. Sci. U. S. A.*, 2010, **107**, 20178–20183.
178 S. T. Belt, F.-W. Grevels, W. E. Klotzbücher, A. McCamley and R. N. Perutz, *J. Am. Chem. Soc.*, 1989, **111**, 8373–8382.
179 H. Hennig, *Coord. Chem. Rev.*, 1999, **182**, 101–123.
180 J. A. Maguire, W. T. Boese and A. S. Goldman, *J. Am. Chem. Soc.*, 1989, **111**, 7088–7093.
181 J. S. Bridgewater, T. L. Netzel, J. R. Schoonover, S. M. Massick and P. C. Ford, *Inorg. Chem.*, 2001, **40**, 1466–1476.
182 A. D. Chowdhury, J. Julis, K. Grabow, B. Hannebauer, U. Bentrup, M. Adam, R. Franke, R. Jackstell and M. Beller, *ChemSusChem*, 2015, **8**, 323–330 and references therein.
183 H. Chen and J. F. Hartwig, *Angew. Chem., Int. Ed.*, 1999, **38**, 3391–3393.
184 T. J. Mazacano and N. P. Mankad, *J. Am. Chem. Soc.*, 2013, **135**, 17258–17261.
185 C. B. Breeter, A. D. Chowhury, R. Adam, R. Jackstell and M. Beller, *Org. Biomol. Chem.*, 2015, **13**, 10336–10340.
186 N. W. Hoffman and T. L. Brown, *Inorg. Chem.*, 1978, **17**, 613–617.
187 D. A. Valyaev, D. Wei, S. Elangovan, M. Cavailles, V. Dorcet, J.-B. Sortais, C. Darcel and N. Lugan, *Organometallics*, 2016, **35**, 4090–4098 and references therein.